

Accelerating Globally Optimal Consensus Maximization in Geometric Vision

Xinyue Zhang, *Student Member, IEEE*, Liangzu Peng, Wanting Xu, *Student Member, IEEE*,
and Laurent Kneip, *Senior Member, IEEE*

Abstract—Branch-and-bound-based consensus maximization stands out due to its important ability of retrieving the globally optimal solution to outlier-affected geometric problems. However, while the discovery of such solutions carries high scientific value, its application in practical scenarios is often prohibited by its computational complexity growing exponentially as a function of the dimensionality of the problem at hand. In this work, we convey a novel, general technique that allows us to branch over an $n - 1$ dimensional space for an n -dimensional problem. The remaining degree of freedom can be solved globally optimally within each bound calculation by applying the efficient interval stabbing technique. While each individual bound derivation is harder to compute owing to the additional need for solving a sorting problem, the reduced number of intervals and tighter bounds in practice lead to a significant reduction in the overall number of required iterations. Besides an abstract introduction of the approach, we present applications to three fundamental geometric computer vision problems: camera resectioning, relative camera pose estimation, and point set registration. Through our exhaustive tests, we demonstrate significant speed-up factors at times exceeding two orders of magnitude, thereby increasing the viability of globally optimal consensus maximizers in online application scenarios.

Index Terms—Consensus Maximization, Branch and Bound, Interval Stabbing, Geometric Vision

1 INTRODUCTION

CONSENSUS Maximization (CM) plays an important role in the field of Geometric Computer Vision. Given a set of pair-wise correspondences, the task is to find a solution that is geometrically consistent. Important examples are given by camera resectioning and epipolar geometry, where we are given input correspondences between 3D world points and 2D image points, or simply 2D image points drawn from two distinct images. However, rather than just having to find an optimal solution to absolute or relative camera pose by minimizing an integral error taken over all correspondences, problems in geometric computer vision are often complicated by the presence of outliers in the data. The majority of solvers employs least sum-of-squares objectives, which are easily disturbed by outliers. In the outlier affected case, the objective is therefore changed to the maximization of the number of correspondences for which the error falls below a pre-defined error threshold, the latter often being chosen as a function of the natural noise in the data. We refer to this as the Consensus Maximization (CM) problem.

Mathematically, the CM problem may be formulated as follows. Let $f : \mathcal{C} \times \mathcal{D} \rightarrow [0, \infty)$ be a residual function derived from the problem to be solved. $\mathcal{C} \subset \mathbb{R}^n$ denotes the constraint set that contains the desired solution variable \mathbf{b}^* , and \mathcal{D} is the data domain containing data samples \mathbf{s}_i . The entire, corrupted set of sample data is given by $S = \{\mathbf{s}_i\}_{i=1}^M \subset \mathcal{D}$. A sample \mathbf{s}_i is determined as an inlier if

$f(\mathbf{b}, \mathbf{s}_i)$ is less or equal to a threshold value ϵ , and an outlier otherwise. The general form of CM is therefore given by the optimization problem

$$\begin{aligned} \max_{\mathbf{b}, \mathcal{I}} \quad & |\mathcal{I}| \\ \text{s.t.} \quad & f(\mathbf{b}, \mathbf{s}_i) \leq \epsilon, \\ & \forall \mathbf{s}_i \in \mathcal{I} \subseteq \mathcal{D} \end{aligned} \quad (1)$$

where $|\cdot|$ denotes the number of elements in a set (cardinality) and \mathcal{I} can be viewed as a set of inliers with respect to \mathbf{b} .

Given the count-based nature of CM, the objective is generally discrete and can no longer be solved using traditional optimization approaches. Instead, there are two kinds of CM approaches that have been proposed over the years: Randomized and deterministic. Randomized consensus maximization employs iterative random sampling of small subsets to generate model hypotheses \mathbf{b} from least-squares solvers. In each iteration, we then find all correspondences for which $f(\mathbf{b}, \mathbf{s}_i) \leq \epsilon$, and thus determine the cardinality of the inlier subset \mathcal{I} that agrees with the calculated hypothesis. If an outlier-free subset is sampled, we tendentially find a good hypothesis and an inlier ratio that is close to the true inlier ratio. Termination criteria typically depend on the expected and current best inlier ratio. The method returns the solution \mathbf{b} corresponding to the largest cardinality inlier subset found during the iterations. Simple as it sounds, randomized CM methods such as RANSAC [1] have been a milestone for robust geometric model estimation, and they are in broad use today. However, Randomized CM suffers from the inability to guarantee global optimality within a finite number of iterations. The expected required number of iterations to sample an outlier-free subset grows exponentially as the outlier ratio increases.

- X. Zhang, W. Xu and L. Kneip are with the Mobile Perception Lab, ShanghaiTech University
E-mails: see <https://mpl.sist.shanghaitech.edu.cn/contact.html>
- L. Peng is with the Center for Innovation in Data Engineering and Science (IDEAS), University of Pennsylvania
Email: lpenn@seas.upenn.edu

This is where Deterministic CM comes into play [2]–[4]. Instead of seeking consensus via randomization, deterministic methods exhaustively search the whole solution space, thereby guaranteeing global optimality. Several paradigms for the global search exist, such as Branch and Bound (BnB) [2], A^* tree search [3], and bisectioning [4], to just name a few. The global search provides an accurate solution and is able to handle extreme outlier ratios. Though computationally demanding, deterministic CM therefore remains of crucial scientific value especially as a reference implementation to test alternative (e.g. randomized) CM methods in scenarios in which no ground truth solution is available (e.g. on real, outdoor data).

This paper addresses the computational efficiency of deterministic CM. We introduce Accelerated deterministic Consensus Maximization (ACM), a novel method that can be widely applied to speed up BnB-based globally optimal CM without depending much on the specific nature of a solved problem. This contribution is important as globally optimal, deterministic methods quickly become computationally intractable as a function of the dimensionality of the problem. The detailed contributions and paper structure are as follows.

1.1 Contributions

- We propose ACM, a general and flexible technique for accelerating deterministic consensus maximization. The method proceeds by performing a 1-DoF reduction of the space over which BnB is branching. The remaining dimension is solved efficiently and globally optimally using interval stabbing.
- The bounds achieved via this technique are not only faster to compute, but also tighter.
- We apply ACM on 4 different problems covering scenarios from 1 dimension to 3 dimension and obtain a $2 \times 100 \times$ speed-up (and sometimes exceeding $300 \times$ speed-up).

1.2 Paper Structure

The rest of this work is organised as follows: Section 2 reviews important related literature on both randomized and deterministic consensus maximization methods as well as existing approaches to increase their computational efficiency. Section 3 reviews the Branch and Bound method in computer vision and the key technique of interval stabbing. Section 4 contains our core contribution: Accelerated Consensus Maximization. It introduces the main technique for 1-DoF dimensionality reduction, requirements for the approach to be applicable, and important properties such as computational complexity. Next, Sections 5, 6, and 7 present applications on the 1-dimensional problem of IMU-supported camera localization, the 2-dimensional problem of relative pose under a planar motion assumption, and the 3-dimensional problems of Correspondence-based and Correspondence-less point set registration, respectively. We conclude with a discussion in Section 8.

2 RELATED WORK

The randomized RANSAC method as proposed by Fischler and Bolles [1] remains the most widely used consensus

maximization algorithm til date. For a collection of several important geometric registration problems that have been embedded into RANSAC, the reader is kindly referred to the OpenGV framework by Kneip and Furgale [5]. Though the focus of this work lies on deterministic CM, it is worth noting a few extensions to RANSAC that have been proposed over the years. Torr and Zissermann [6] propose MLESAC, a variation that sums up inlier likelihoods during the inlier verification stage rather than just a count based on a fixed inlier threshold. Nistér [7] introduces preemptive RANSAC, a variation that first generates many hypotheses and verifies them against a subset of the correspondences to eliminate wrong models. The remaining hypotheses are verified against a gradually larger subset of the correspondences while continuing to remove wrong models. Only very few hypotheses have to be verified against all data samples, and the strongest one survives. Chum et al. [8] propose LO-RANSAC, a variant that includes local optimization in each iteration, and thereby helps to validate the typical assumption that any outlier-free sample can lead to a model that agrees with all inliers. Later, Chum and Matas [9] propose PROSAC. Unlike RANSAC, samples are not treated equally but drawn from a progressively larger subset of the original correspondences, the latter being ordered by matching quality. Based on the assumption that higher matching scores lead to better correspondences, the algorithm potentially achieves orders of magnitude speed-up. More recently, Barath and Matas [10] propose Graph-cut Ransac (GC-RANSAC). Similar to MLESAC, the method employs a probabilistic kernel to map distances onto the interval $[0, 1]$ and sums up those values during the inlier verification stage. However, GC-Ransac additionally relies on the assumption of spatial proximity of inliers and outliers, and employs graph-cut for a globally optimal solution of the labelling problem.

While not addressing CM, it is worth listing early works using branch-and-bound for the globally optimal solution of geometric fitting problems as several important techniques for later deterministic CM approaches are gained from here. Olsson et al. [11] and Hartley and Kahl [12], [13] find geometrically globally optimal solutions to 2D-3D correspondence-based camera resectioning, a problem to which previous solvers exclusively employed algebraic error residuals. The solutions also go beyond previous globally optimal solvers as they are the first to enable guaranteed geometric optimality over the space of rotations. In particular, the method of Hartley and Kahl [12], [13] is faster and introduces important bounding operations enabling branching over the space of rotations, a technique that proves valuable for many of the following spatial registration-based CM problems. By employing the ℓ_∞ norm, they furthermore propose the first geometrically globally optimal solution to the relative camera pose problem. Olsson et al. [14] propose further branch-and-bound based geometrically globally optimal solutions to point, line, and plane based Euclidean 3D-3D registration as well as 3D-2D registration. The work introduces the technique of convex underestimators in combination with branch-and-bound, which later finds reuse in CM. The work claims that it simply needs convex sets to which points are registered, and thus hints at potential use in correspondence-less scenarios. However,

in practice the convex sets consist of a single landmark, hence correspondence-free or outlier-affected scenarios are not yet addressed. Although slightly less related, it is worth mentioning that globally optimal solutions in the space of Euclidean transformations under an algebraic error criterion have later been derived using relaxations of Quadratically Constrained Quadratic Programs (QCQP) [15], [16].

Back to CM, an interesting method able to digest a limited amount of outliers is presented by Kahl et al. [17], who propose a global branch-and-bound based minimization of the L1-norm of the residual vector for triangulation and uncalibrated pose estimation. The branch-and-bound method remains the pre-dominant choice for deterministic variants. The seminal work of Li [2] provides a general framework for solving problems that can be formulated using Direct Linear Transformation (e.g. line-fitting, essential matrix fitting). The work describes the problem as a bilinear program, and relaxes it to a convex underestimator in the form of a linear program by assuming bounds on the searched transformation. A globally optimal solution is then found by embedding the program into a branch-and-bound scheme. Later, Bazin et al. [18] introduce deterministic CM solutions to the problem of pure rotation estimation for panorama stitching, rotating lidar point set registration, and line clustering with vanishing point estimation. In their later work, they extend the pure rotation determination to the uncalibrated case [19]. An improved method for vanishing point estimation has recently been presented by Li et al. [20]. Yang et al. [21] extend the DLT-based method of Li [2] for robust, deterministic essential matrix fitting by branching over a minimal 5D essential matrix manifold parametrization. In their work, they reuse the rotation space branching method of Hartley and Kahl [13]. The conceptually simpler robust correspondence-based point set registration is only introduced later [22]. Speciale et al. [23] introduce CM with linear inequality constraints.

More recently, we have seen a number of solutions for correspondence-based globally optimal vision-based relative pose estimation under a constrained motion model. Liu et al. [24] address the case of known gravity, and Jiao et al. [25] utilize prior knowledge about the roll and pitch angles from a nearby reference pose. They furthermore decouple yaw and translation estimation, and employ a maximum clique estimator for the latter. Liu et al. [26] propose solutions for planar ground vehicle motion, respectively. Jiao et al. [27] again employ translation invariant features and IMU readings in order to reduce the rotation search to a one-directional search. Above methods achieve a substantial speed-up by assuming prior knowledge and reducing the dimensionality of the branching space.

Deterministic CM has also been applied in situations in which data correspondences are not given upfront, but have to be found as a by-product of the optimization. An early seminal contribution is made by Breuel [28], who proposes solutions to globally optimal correspondence-less matching of points under a Euclidean transformation in the image plane. Later, by using inlier cardinality maximization and branching over 3D rotations, Yang et al. [29], [30] solve globally optimally for pose and correspondence towards 3D point set registration. Their method—denoted Go-ICP—speeds up the estimation by adding local optimization to the

lower bound calculation, thereby accelerating the pruning of branches inside BnB. Bustos et al. [31] propose fast correspondence-less point set registration by creating possible match lists from stereo-graphic projections. Liu et al. [32] propose simplified globally-optimal point set registration by creating hypothetical match-lists from rotation invariant features. Similar highly efficient point-set registration methods have recently been proposed by Yang et al. [33], [34]. Cai et al. [35] address the globally optimal 4D point set registration problem given by using lidar scanners with built-in level compensation. A highly efficient method for 3D point-based rotation and correspondence is presented in [36], which is highly related to our method as it also makes use of interval stabbing in order to achieve a very substantial improvement in computational efficiency. Campbell et al. [37], [38] finally propose a globally optimal solution to simultaneous camera pose and correspondence determination under a geometric error criterion, again branching over the space of rotations. Later, Campbell et al. [39] propose a related method in which a spherical 3D mixture-model describing the 3D spatial location of landmarks (e.g. objects) is aligned globally optimally with a 2D mixture-model describing the 2D image-based location of their projections (e.g. semantic segments). Hu and Kneip [40] propose an interesting variation of the globally optimal correspondence-free point set registration problem in which they jointly solve for a symmetry plane, thereby enabling good performance in situations of extremely low overlap. Gao et al. [41] again propose a method for globally optimal correspondence-free registration of points in the image plane under a constrained, non-holonomic transformation model. The method is successfully applied to a down-ward facing camera mounted on an Ackermann-steering vehicle for planar motion determination. Peng et al. [42], [43] finally apply the globally optimal branch-and-bound technique to contrast maximization-based event camera motion estimation.

Whilst alternative techniques based on tree-search [3], [44], [45] and bi-convex programming [4], [45] exist, CM remains a hard problem [46]. The present paper focuses on the predominant technique of branch-and-bound-based deterministic CM and the question how to increase its computational efficiency. However, in contrast to many existing solutions that employ problem-dependent techniques such as prior knowledge, algebraic manipulations, or invariant representations, our proposed method uses interval stabbing for a general speed-up of the original problem solution.

3 PRELIMINARIES

Before introducing our accelerated CM method, a few preliminaries on interval analysis, the plain branch and bound algorithm, and interval stabbing need to be covered.

3.1 Interval Analysis

We summarize some basics of interval operations (see [47]):

Corollary 1 (Interval Arithmetic). *Let $X = [a, b]$ and $Y = [c, d]$ be two intervals, Then*

$$\begin{aligned} X + Y &= [a + c, b + d] \\ X - Y &= [a - d, b - c] \end{aligned}$$

$$\begin{aligned}
X \cdot Y &= [\min\{ac, ad, bd, bd\}, \\
&\quad \max\{ac, ad, bc, bd\}] \\
X/Y &= [a, b] \cdot [1/d, 1/c] \text{ if } c > 0 \\
\min\{X, Y\} &= [\min\{a, c\}, \min\{b, d\}] \\
\max\{X, Y\} &= [\max\{a, c\}, \max\{b, d\}]
\end{aligned}$$

Definition 1 (Interval Mapping). Let X be an interval. Then the interval operation is defined by

$$f(X) := \{f(x) : x \in X\} = [\min_{x \in X} f(x), \max_{x \in X} f(x)], \quad (2)$$

where $f : X \rightarrow \mathbb{R}$ denotes a continuous function such that $f(X)$ is an interval.

3.2 Branch and Bound

As shown in [28], Branch and Bound (BnB) is a deterministic paradigm commonly used to maximise consensus and find the global optimum of geometric computer vision problems. The main idea of BnB is to recursively branch over the solution space and calculate bounds for the maximum cardinality of the inlier subset on all candidate sub-regions, then prune cubes whose upper bound is smaller than the maximal lower bound so far. The algorithm keeps splitting cubes until the bounds are sharp enough, i.e. the lower bound is close to the upper bound. Generally speaking, the optimality of BnB stems from the fact that it is an exhaustive search method that uses bounding operations to prune useless branches. However, BnB gains efficiency over a brute-force search by pruning useless branches (i.e. potentially large sub-regions) at an early stage without having to examine all sub-regions down to the leaf level.

Algorithm 1 presents a basic BnB pipeline using Best-First-Search. It consists of several ingredients: cube initialization (line 1), cube subdivision (line 16), lower bounding operation (lines 3 and 8), and upper bounding operation (lines 4 and 17). Each of these steps is introduced in the following.

Cube Initialization. Cube Initialization (line 1, Algorithm 1) refers to constructing an initial cube or hypercube $C_0 \subset \mathbb{R}^n$, over which the BnB algorithm searches for the global optimum of the consensus maximization objective (1). C_0 should therefore be chosen such that it actually contains the global optimum. Usually, this can be done fairly easily by considering the nature of the solved problem or the data distribution. For example, one can set $[-\pi, \pi]$ as the initial 1-dimensional cube for an angular search.

Cube Subdivision. In each iteration (line 6, Algorithm 1), BnB takes a cube or hypercube

$$C = [c_1^l, c_1^r] \times \dots \times [c_n^l, c_n^r] \subset \mathcal{C} \subseteq \mathbb{R}^n,$$

from the priority queue (line 7) and splits it into smaller ones (line 16). The splitting rule is typically chosen such that a cube is divided into 2^n congruent sub-cubes. In practice, in order to balance accuracy and running time, additional stopping criteria are used such as limiting the maximal splitting depth d or setting a tolerance τ that limits the minimal diameter of the sub-cubes.

BnB - Lower Bound. Given the current cube C taken from the priority queue (line 7), we define its centre point \mathbf{b}_c as

$$\mathbf{b}_c = [(c_1^l + c_1^r)/2, \dots, (c_n^l + c_n^r)/2]^T.$$

Algorithm 1 Branch and Bound

Input: Dataset $\mathcal{S} = \{\mathbf{s}_i\}_{i=1}^N$, threshold ϵ

Output: Best solution \mathbf{b}^*

```

1:  $C_0 \leftarrow \text{CubeInitialization}$ 
2:  $q \leftarrow$  initialize an empty priority queue
3:  $L^*, \mathbf{b}^* \leftarrow \text{getLowerBound}(C_0, \mathcal{S}, \epsilon)$ 
4:  $U(C_0) \leftarrow \text{getUpperBound}(C_0, \mathcal{S}, \epsilon)$ 
5: insert  $C_0$  into  $q$  with priority  $U(C_0)$ 
6: while  $q$  is not empty do
7:   pop  $C$  from  $q$  with the largest upper bound
8:    $L(C), \mathbf{b} \leftarrow \text{getLowerBound}(C, \mathcal{S}, \epsilon)$ 
9:   if  $L^* < L(C)$  then
10:     $L^* \leftarrow L(C)$ 
11:     $\mathbf{b}^* \leftarrow \mathbf{b}$ 
12:   end if
13:   if  $U(C) == L^*$  then
14:     return  $\mathbf{b}^*$ 
15:   else if  $U(C) > L^*$  then
16:     for  $C_i$  in  $\text{splitCube}(C)$  do
17:        $U(C_i) \leftarrow \text{getUpperBound}(C_i, \mathcal{S}, \epsilon)$ 
18:       insert  $C_i$  into  $q$ 
19:     end for
20:   else
21:     discard  $C$ 
22:   end if
23: end while
24: return  $\mathbf{b}^*$ 

```

Then, a trivial lower bound of (1) over C arises as the number of points that satisfy $0 \leq f(\mathbf{b}_c, \mathbf{s}_i) \leq \epsilon$, since for an arbitrary \mathbf{b} and the global optimum \mathbf{b}^* it is always true that

$$\sum_{i=1}^N \mathbf{1}(f(\mathbf{b}, \mathbf{s}_i) < \epsilon) \leq \sum_{i=1}^N \mathbf{1}(f(\mathbf{b}^*, \mathbf{s}_i) < \epsilon). \quad (3)$$

This calculation of the lower bound happens in line 8. Note that any point in the cube C defines a valid lower bound, and the centre point is chosen for the sake of convenience.

BnB - Upper Bound. An upper bound is typically obtained by relaxing the constraint. Let C be a given cube and let f be the constraint function for which the bounds of f over C can be computed using interval analysis (Corollary 1). Without loss of generality, denote the lower and upper bounds of f at \mathbf{s}_i over C as f_i^l and f_i^r , that is

$$f_i^l \leq f(C, \mathbf{s}_i) \leq f_i^r. \quad (4)$$

Let us recall the constraint in (1) and the characteristics of residuals, i.e. $0 \leq f(\mathbf{b}, \mathbf{s}_i) < \epsilon$. Then the situation when there is no valid solution \mathbf{b} in cube C happens when $f_i^l > \epsilon$ or $f_i^r < 0$. Therefore, through counting points that provide an interval that may contain a solution, we can get a valid upper bound for the summation as follows:

$$\begin{aligned}
\max_{\mathbf{b}} \sum_i \mathbf{1}(f(\mathbf{b}, \mathbf{s}_i) < \epsilon) &\leq \sum_i \mathbf{1}([f_i^l, f_i^r] \cap [0, \epsilon]) \\
&= \sum_i \mathbf{1}(f_i^l \leq \epsilon \text{ and } f_i^r \geq 0). \quad (5)
\end{aligned}$$

The relaxation is achieved by the fact that valid solution intervals all contribute to the inlier count though in reality they may not intersect with each other. Note that, once upper and lower bounds f_i^l and f_i^r have been derived for each i , the integral upper bound (5) can be derived in linear time.

3.3 Interval Stabbing

Suppose we are given a set of intervals $\mathcal{X} = \{[x_i^l, x_i^r]\}_{i=1}^L$. The problem of interval stabbing aims to find the maximal subset of intervals \mathcal{I} that are intersecting with each other, or in a more figurative way, that could be stabbed by a stabber $s \in \mathbb{R}$. It can be formulated as follows

$$\begin{aligned} \max_{s, \mathcal{I}} \quad & |\mathcal{I}| \\ \text{s.t.} \quad & s \in [x_i^l, x_i^r], \\ & \forall [x_i^l, x_i^r] \in \mathcal{I} \subseteq \mathcal{X}. \end{aligned} \quad (6)$$

The problem of Interval Stabbing (IS) (6) can simply be solved in $\mathcal{O}(L \log L)$ time and $\mathcal{O}(L)$ space as presented in algorithm 2. It was studied in [48] as a subproblem of windowing queries that can be deterministically and efficiently solved using advanced data structures, such as interval trees, segment trees and priority trees. Adaptive voting generalized from histogram voting has a similar idea but its time complexity is $\mathcal{O}(L^2)$ [25], [27], [33], [34]. In recent practices, IS is found to be a powerful tool in optimization [20], [22], [35], [36]. In particular, [20], [35], [36] used Interval Stabbing to efficiently solve an inner problem, an indicative example of how Interval Stabbing can help to accelerate algorithms.

Algorithm 2 Interval Stabbing

Input: Intervals $\mathcal{X} = \{[x_i^l, x_i^r]\}_{i=1}^L$
Output: Best Stabber s , #Stabbed intervals $nStabbed$

```

1:  $I \leftarrow$  Sort all the endpoints in  $\mathcal{X}$ 
2:  $n \leftarrow 0, count \leftarrow 0$ 
3: for  $i = 1$  to  $2L$  do
4:   if  $I(i)$  is an left endpoints then
5:      $count \leftarrow count + 1$ 
6:     if  $count > n$  then
7:        $nStabbed \leftarrow count$ 
8:        $s \leftarrow I(i)$ 
9:     end if
10:  else
11:     $count \leftarrow count - 1$ 
12:  end if
13: end for
14: return  $s, nStabbed$ 
```

4 ACCELERATED CONSENSUS MAXIMIZATION

In this section, we present our method Accelerated Consensus Maximization (ACM). Instead of searching in the original n -dimensional space, ACM searches and branches over an $n - 1$ dimensional space, and uses IS to deal with the remaining variable. Implementation-wise, ACM uses the

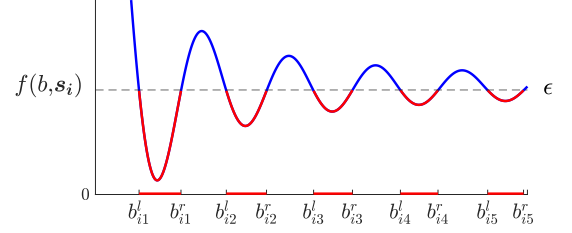


Fig. 1: A visual example of (8): Given a threshold ϵ and sample s_i , in general one can find a disjoint union of intervals (red, x -axis) for which every point b satisfies $f(b, s_i) \leq \epsilon$.

same BnB diagram as shown in Algorithm 1. However, different from BnB, in line 1, ACM initializes an $(n - 1)$ -dimensional cube. In line 8 and 17, it devises the ACM bounding operations. The main modification of ACM lies in adjusting the bounding operations to an $(n - 1)$ -dimensional cube. In the following, we will first introduce the general idea of ACM and then show its global optimality. Finally, we analyze its time complexity. For a more intuitive understanding, we use plain BnB to refer to the standard BnB mentioned above. Note that the general idea here is to provide a basic intuition about ACM, details may differ for specific problems.

4.1 Core of The Method

Consider the 1-dimensional Consensus Maximization problem as follows

$$\begin{aligned} \max_{b \in \mathbb{R}, \mathcal{I}} \quad & |\mathcal{I}| \\ \text{s.t.} \quad & f(b, s_i) \leq \epsilon, \\ & \forall s_i \in \mathcal{I} \subseteq \mathcal{D}. \end{aligned} \quad (7)$$

For each sample s_i , the properly defined constraint function f can be used to inversely find the union of all the possible intervals of b

$$f(b, s_i) \leq \epsilon \Leftrightarrow b \in \bigcup_j [b_{i,j}^l, b_{i,j}^r]. \quad (8)$$

A visual example is given in Fig. 1.

Merging the intervals if necessary, we could assume all intervals $[b_{i,j}^l, b_{i,j}^r]$ in (8) are disjoint. This suggests that (7) can be reformulated as an Interval Stabbing problem as in (6). In this way, we get the key observation: *1-dimensional Consensus Maximization can be directly solved by Interval Stabbing*, which finds a globally optimal solution BnB without iteratively searching the solution space as plain BnB does. Note that, for the convenience of the discussion, in the following, we will suppose that the solution of $f(b, s_i) < \epsilon$ will lead to only one interval instead of a union of intervals as illustrated in (8). Note that this notion-wise simplification does not affect the implementation. Having a union of intervals would simply mean that interval stabbing would have to be executed over additional intervals.

Let us now proceed by generalizing the above observation to the n -dimensional Consensus Maximization problem. Recall the general consensus maximization problem (1). Plain BnB solves it by searching \mathbf{b} over an n -dimensional space. We propose Accelerated Consensus Maximisation (ACM) to search $n - 1$ variables of \mathbf{b} and use Interval

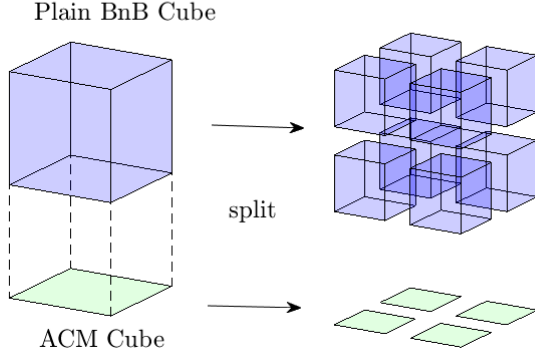


Fig. 2: Search spaces of plain BnB (blue, top row) and ACM (green, bottom row). The left column shows example volumes and the right column the corresponding subcubes after splitting. Plain BnB splits an n -dimensional cube into 2^n sub-cubes. ACM splits an $(n - 1)$ -dimensional cube into 2^{n-1} sub-cubes.

Stabbing to solve for the remaining 1 variable. As illustrated in Fig. 2, benefitting from the lower-dimensional search space, ACM branches over a conceivably smaller number of sub-cubes which makes it converge significantly faster than plain BnB. Denote $\mathbf{b} = [b_1, b_2, \dots, b_n]^T$. Without loss of generality, we assume ACM branches over the first $n - 1$ variables in \mathbf{b} , and we denote them as $\mathbf{b}_{1:n-1}$. Let \mathcal{C}_{plain} represent a plain BnB cube in n -dimensional space and \mathcal{C}_{ACM} represent the corresponding ACM cube in $(n - 1)$ -dimensional space. As visualized in Fig. 2, \mathcal{C}_{ACM} can be seen as \mathcal{C}_{plain} less the last dimension. Next, let us introduce a general function representation for $f(\mathbf{b}|s_i)$ in which b_n is conveniently separated from $\mathbf{b}_{1:n-1}$. It is given by

$$f(\mathbf{b}|s_i) = \sum_j f_j(b_n, h_j(\mathbf{b}_{1:n-1})|s_i), \quad (9)$$

where both f_j and h_j depend on the samples s_i .

To implement the above intuition of ACM, we need to answer two questions:

- (ACM - Union) Once $\mathbf{b}_{1:n-1}$ is given, how to invert the constraint function f to obtain the interval(s) $[b_{ni}^l, b_{ni}^r]$ in analogy to (8)?
- (ACM - Bounds) How to derive the lower and upper bounds of the objective for ACM (recall that ACM is a BnB-based method)?

For (ACM - Union), we could in principle find all roots of $(\sum_j f_j(b_n, h_j(\mathbf{b}_{1:n-1})|s_i)) - \epsilon = 0$ over b_n using numerical methods and then recover the intervals $[b_{ni}^l, b_{ni}^r]$ from here. However, in most practical scenarios, we can solve this equation in closed form. Such closed form is problem-specific, so we will not discuss it at this moment and we will instead give concrete examples later.

Computing (ACM - Bounds) is slightly more complicated. However, as we will next show, mild assumptions on the form of the function $f(\mathbf{b}|s_i)$ will again enable us to reuse Interval Stabbing and solve for one dimension optimally while branching over the remaining $n - 1$ variables.

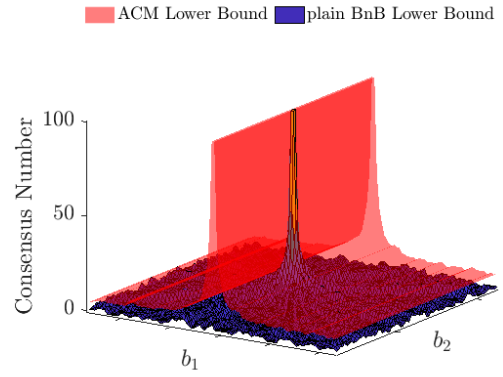


Fig. 3: Visualization of the lower bounds of plain BnB and ACM on a 2-dimensional example. Plain BnB branches to search two variables b_1 and b_2 . ACM searches over the space of b_1 , and uses interval stabbing to determine b_2 . The red curves are higher, i.e., the lower bounds of ACM are tighter.

ACM - Lower Bound. As explained above, for any $\mathbf{b}_{1:n-1} \in \mathcal{C}_{ACM}$ given, we can manage to find the interval of b_n on each data sample s_i

$$f(b_n|\mathbf{b}_{1:n-1}, s_i) \leq \epsilon \Rightarrow b_n \in [b_{ni}^l, b_{ni}^r]. \quad (10)$$

Therefore, a valid lower bound can be found by doing Interval Stabbing on $\{[b_{ni}^l, b_{ni}^r]\}_{i=1}^M$

$$\begin{aligned} L(\mathcal{C}_{ACM}) &:= \max_{b_n} \sum_i \mathbf{1}(f(b_n|\mathbf{b}_{1:n-1}, s_i) \leq \epsilon) \\ &= \max_{b_n} \sum_i \mathbf{1}(b_n \in [b_{ni}^l, b_{ni}^r]) \\ &\leq \max_{\mathbf{b}} \sum_i \mathbf{1}(f(\mathbf{b}, s_i) \leq \epsilon), \end{aligned} \quad (11)$$

where the inequality here is derived by the fact that a randomly chosen $\mathbf{b}_{1:n-1}$ will always be worse or equal to the best solution $\mathbf{b}_{1:n-1}^*$. Note that, interestingly, for the same problem the lower bound of ACM is tighter than the trivial lower bound of plain BnB as visualized in Fig. 3:

$$\begin{aligned} L(\mathcal{C}_{ACM}) &= \max_{b_n} \sum_i \mathbf{1}(b_n \in [b_{ni}^l, b_{ni}^r]) \\ &\geq \sum_i \mathbf{1}(f(\mathbf{b}, s_i) \leq \epsilon) = L(\mathcal{C}_{plain}) \end{aligned} \quad (12)$$

for any $\mathbf{b} \in \mathcal{C}_{plain}$ (with $\mathbf{b}_{1:n-1}$ fixed).

ACM - Upper Bound. Next, let us assume that all $f_j(b_n, h_j(\mathbf{b}_{1:n-1})|s_i)$ are monotonically increasing in $h_j(\mathbf{b}_{1:n-1})$. This is a mild assumption as 1) monotonicity is only needed over the interval of $h_j(\mathbf{b}_{1:n-1})$ for $\mathbf{b}_{1:n-1} \in \mathcal{C}_{ACM}$, and that interval is decreasingly small as branching proceeds, and 2) the following derivations are equally simple to derive if some or all of the $f_j(b_n, h_j(\mathbf{b}_{1:n-1})|s_i)$ are monotonically decreasing in $h_j(\mathbf{b}_{1:n-1})$, so in fact, monotonicity alone is a sufficient condition for the derivation.

After properly bounding the internal functions h_j on \mathcal{C}_{ACM} using Interval Arithmetic (Corollary 1), we can get

$$h_{ij}^l \leq h_j(\mathcal{C}_{ACM}|s_i) \leq h_{ij}^r, \quad (13)$$

for each sample s_i . Then, on \mathcal{C}_{ACM} the general constraint (1) along with the basic characteristics of residuals translates into

$$\begin{aligned} 0 &\leq \sum_j f_j(b_n, h_j(\mathcal{C}_{ACM})|s_i) < \epsilon \\ \Leftrightarrow &[\sum_j f_j(b_n, h_{ij}^l|s_i), \sum_j f_j(b_n, h_{ij}^r|s_i)] \cap [0, \epsilon]. \end{aligned} \quad (14)$$

Again considering the first $n - 1$ variables as given, interval (14) can be relaxed as follows

$$\begin{cases} \sum_j f_j(b_n|s_i, h_{ij}^l) \leq \epsilon \\ \sum_j f_j(b_n|s_i, h_{ij}^r) \geq 0, \end{cases} \quad (15)$$

and using either numerical or closed-form analytical solutions, these inequalities can again be resolved to identify valid intervals $b_n \in [\bar{b}_{ni}^l, \bar{b}_{ni}^r]$ for each sample s_i . A valid upper bound of ACM can be found by doing Interval Stabbing on these intervals, thus resulting in the following upper bound

$$\begin{aligned} U(\mathcal{C}_{ACM}) &:= \max_{b_n} \sum_i \mathbf{1}(b_n \in [\bar{b}_{ni}^l, \bar{b}_{ni}^r]) \\ &\geq \max_{\mathbf{b}} \sum_i \mathbf{1}(f(\mathbf{b}, s_i) \leq \epsilon). \end{aligned} \quad (16)$$

Again note that the requirement of monotonicity is not a severe limitation. Monotonicity is only required on the sub-region on which the current bounds are evaluated. In practice, it is very often possible to achieve at least piece-wise monotonicity even for more complicated, non-linear functions.

For better illustration, we provide two kinds of constraint function f and introduce how to separate b_n out.

Example 1. Suppose $f(\mathbf{b}, s_i)$ can be decomposed as the addition of two parts as

$$f(\mathbf{b}, s_i) = h_1(\mathbf{b}_{(1:n-1)}|s_i) + g_2(b_n|s_i). \quad (17)$$

For any \mathcal{C}_{ACM} given, we can manage to find the interval of $h_1(\mathcal{C}_{ACM}|s_i)$

$$h_{i1}^l \leq h_1(\mathcal{C}_{ACM}|s_i) \leq h_{i1}^r. \quad (18)$$

Then, as discussed for the common upper bound of plain BnB, we can relax the objective of CM by counting the possible intervals as follows

$$\begin{aligned} &[h_{i1}^l + g_2(b_n|s_i), h_{i1}^r + g_2(b_n|s_i)] \cap [0, \epsilon] \\ \Leftrightarrow &g_2(b_n|s_i) \in [-h_{i1}^r, \epsilon - h_{i1}^l] \\ \Rightarrow &b_n \in [\bar{b}_{ni}^l, \bar{b}_{ni}^r], \end{aligned} \quad (19)$$

where we can deduce an interval of b_n on \mathcal{C}_{ACM} for each data sample s_i . Therefore, a valid upper bound can be found by doing Interval Stabbing on $\{[\bar{b}_{ni}^l, \bar{b}_{ni}^r]\}_{i=1}^M$, i.e.

$$U(\mathcal{C}_{ACM}) := \max_{b_n} \sum_i \mathbf{1}(b_n \in [\bar{b}_{ni}^l, \bar{b}_{ni}^r]). \quad (20)$$

Example 2. Suppose $f(\mathbf{b}, s_i)$ can be decomposed as the multiplication of two parts as

$$f(\mathbf{b}, s_i) = h_1(\mathbf{b}_{(1:n-1)}|s_i) \cdot g_1(b_n|s_i). \quad (21)$$

For any \mathcal{C}_{ACM} given, we can manage to find the interval of $h_1(\mathcal{C}_{ACM}|s_i)$

$$h_{i1}^l \leq h_1(\mathcal{C}_{ACM}|s_i) \leq h_{i1}^r, \quad (22)$$

and to find a finite range interval for g_1 we suppose that $h_{i1}^l > 0$. Without loss of generality, suppose $g_1(b_n|s_i)$ is greater or equal to zero. Again, we can relax the objective of CM by counting the possible intervals as follows

$$\begin{aligned} &[h_{i1}^l \cdot g_1(b_n|s_i), h_{i1}^r \cdot g_1(b_n|s_i)] \cap [0, \epsilon] \\ \Leftrightarrow &g_1(b_n|s_i) \in [0, \epsilon/h_{i1}^l] \\ \Rightarrow &b_n \in [\bar{b}_{ni}^l, \bar{b}_{ni}^r]. \end{aligned} \quad (23)$$

A valid upper bound is again found by doing Interval Stabbing on $\{[\bar{b}_{ni}^l, \bar{b}_{ni}^r]\}_{i=1}^M$.

Sections 5, 6, and 7 will apply ACM to concrete geometric problems which will further explain its practical usage.

4.2 Time Complexity Analysis

Knowing that plain BnB and ACM are both globally optimal, let us proceed to compare their computational efficiency and analyse which one potentially converges faster to the global optimum. Note that, to compute upper and lower bounds at each iteration, plain BnB uses $\mathcal{O}(M)$ time, while ACM invokes the Interval Stabbing subroutine and therefore consumes $\mathcal{O}(M \log M)$ time. The extra $\log M$ factor appears as a slight disadvantage for ACM, but is in fact the cost that ACM pays for tremendous benefits: ACM is required to branch over a smaller space and yields tighter bounds, resulting in convergence within significantly fewer iterations. The following basic proposition mathematically consolidates our claim:

Proposition 1. *Run the plain BnB (resp. ACM) algorithm with the splitting rule that divides cubes into 2^n (resp. 2^{n-1}) congruent sub-cubes and with the stopping criterion that terminates at the maximal splitting depth d . Then the following holds:*

- (Perfect Bounds) *If at every iteration both ACM and plain BnB prune all sub-cubes except one that contains the global optimum, then ACM needs $\mathcal{O}(2^{n-1})$ iterations to terminate, while plain BnB needs $\mathcal{O}(2^n)$.*
- (Invalid Bounds) *If neither ACM nor plain BnB prunes any sub-cubes at each iteration, then ACM needs $\mathcal{O}(2^{(n-1)d})$ iterations to terminate, while plain BnB needs $\mathcal{O}(2^{nd})$.*

Here we give a numerical feeling of Proposition 1:

Example 3 (Invalid Bounds). Suppose the bounds of ACM and plain BnB are invalid in the sense of Proposition 1. If $n = 3$ and $d = 10$, then ACM terminates in roughly 2^{30} iterations, and plain BnB in 2^{30} . We furthermore have $2^{30}/2^{20} = 1024$, implying that ACM can be 1024 times faster than plain BnB (ignoring the extra $\log M$ factor of ACM due to Interval Stabbing).

Proposition 1 suggests that if the upper and lower bounds for two algorithms are *perfect*, ACM exhibits a minor advantage over plain BnB with a speedup factor of 2, which will be compromised by the extra $\log M$ factor of invoking Interval Stabbing at every iteration. On the other hand, if

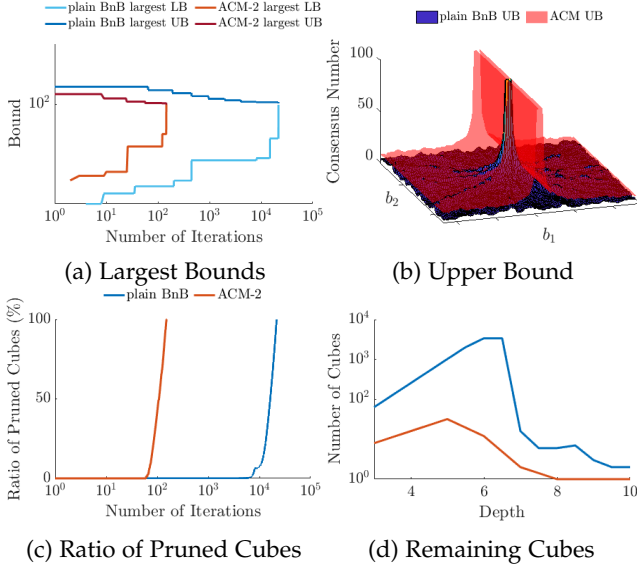


Fig. 4: Visual comparative analysis of ACM: The *largest* upper and lower bounds of ACM are tighter (4a); the upper bounds of ACM and plain BnB are comparable (4b); ACM prunes a higher percentage of cubes in earlier stages (4c); ACM maintains much fewer cubes during execution (4d).

the bounds are *invalid* such that no cubes will be ruled out, then ACM will terminate exponentially faster than plain BnB, with a speedup factor of 2^d ; this advantage of ACM makes its extra $\log M$ term insignificant.

The scenarios of perfect and invalid bounds of Proposition 1 are ideal; in practice, the bounds are neither perfect nor invalid. That said, ACM is preferred for two reasons:

- It is known that deriving tight lower and upper bounds is crucial but difficult for BnB-based methods, and many existing bounds tend to be “invalid” rather than “perfect” [47], [49]. Therefore, acceleration via ACM-based global optimization usually takes place.
- As illustrated in Fig. 3, the bounds that we derive for ACM are based on Interval Stabbing and are more effective in pruning sub-optimal cubes than the usual bounds of plain BnB.

Fig. 4 illustrates the practical benefits of ACM. It is shown in Fig. 4a that the *largest* lower bound of ACM is far tighter than the one of plain BnB; this is a theoretical consequence of the lower bounding operation of ACM being tighter, as explained earlier (see Fig. 3). Interestingly, Fig. 4a shows that the *largest* upper bound of ACM is also tighter, even though the upper bounding operation of ACM is not necessarily better (Fig. 4b). While this phenomenon seems to be contradictory at first glance, it is attributed to two factors: ACM has fewer sub-cubes as it branches over a smaller space; ACM also prunes more sub-cubes due to its tighter lower bounds (Fig. 4c). In other words, ACM essentially calculates the largest upper bound over significantly fewer remaining sub-cubes (Fig. 4d), which is why its largest upper bound is also tighter.

Remark 1. We use the maximal depth as a practical stopping criterion. Intuitively, setting a tolerance for the minimal diameter

of sub-cubes seems more reasonable when comparing plain BnB and ACM. However, it can be shown that the same diameter tolerance approximately implies the same maximal depth. See the appendix for a more detailed explanation.

5 ACM-0: 3D-2D REGISTRATION

Firstly, we would like to introduce ACM concretely by solving a 1-dimensional Consensus Maximization problem: Visual Inertial localization. This problem arises naturally in navigation systems, and aims at solving absolute camera pose from a set of 3D-2D correspondences given prior angular information provided by an Inertial Measurement Unit (IMU). Jiao et al. [27] propose a 1-dimensional plain BnB algorithm to solve it globally optimally.

Problem formulation. Consider a set of 3D-2D correspondences $\{(\mathbf{p}_i, \mathbf{u}_i)\}_{i=1}^M$, where $\mathbf{p}_i \in \mathbb{R}^3$ is a 3D point in world coordinates and $\mathbf{u}_i \in \mathbb{R}^2$ is a 2D image point. The correspondences follow an underlying absolute pose transformation constraint depending on $\mathbf{R}^* \in SO(3)$ and $\mathbf{t}^* \in \mathbb{R}^3$. It is given by

$$\mathbf{u}_i = \pi(\mathbf{R}^* \mathbf{p}_i + \mathbf{t}^*) \quad (24)$$

where $\pi : \mathbb{R}^3 \rightarrow \mathbb{R}^2$ denotes the camera projection function. When camera calibration is known, \mathbf{u}_i simply denotes the normalized image coordinates, and—using the homogeneous representation $\tilde{\mathbf{u}}_i = [\mathbf{u}_i^T, 1]^T$ —(24) becomes the homogeneous equality constraint (omitting noise)

$$\tilde{\mathbf{u}}_i \propto \mathbf{R}^* \mathbf{p}_i + \mathbf{t}^*. \quad (25)$$

Using $\mathbf{R}^* = [\mathbf{r}_1^T, \mathbf{r}_2^T, \mathbf{r}_3^T]^T$, $\mathbf{t}^* = [t_1, t_2, t_3]^T$ and $\mathbf{u}_i = [u_{i1}, u_{i2}]^T$, (25) results in the two simple equality constraints

$$\begin{cases} u_{i1} = \frac{\mathbf{r}_1^T \mathbf{p}_i + t_1}{\mathbf{r}_3^T \mathbf{p}_i + t_3} \\ u_{i2} = \frac{\mathbf{r}_2^T \mathbf{p}_i + t_2}{\mathbf{r}_3^T \mathbf{p}_i + t_3} \end{cases}. \quad (26)$$

Representing the rotation \mathbf{R}^* in angular form, we have

$$\mathbf{R}^* = \mathbf{R}_z^*(\alpha^*) \mathbf{R}_y^*(\beta^*) \mathbf{R}_x^*(\gamma^*), \quad (27)$$

where $\alpha^*, \beta^*, \gamma^* \in [-\pi, \pi]$ are the rotation angles along the z , y , and x axis, respectively. Assuming β and γ can be estimated from inertial measurements (i.e. an IMU), only 4 unknowns remain in the linear equations (26). Therefore, with 2 pairs of correspondences $(\mathbf{p}_i, \mathbf{u}_i)$ and $(\mathbf{p}_j, \mathbf{u}_j)$, we can obtain 4 equations to produce a unique solution. Using Translation Invariant Measurements (TIM) as proposed in [27], we can simplify the aforementioned 4 equations to eliminate translation and arrive at a single equation that only relates the unknown angle α

$$d(\alpha^*)^{(ij)} := d_1^{(ij)} \sin \alpha^* + d_2^{(ij)} \cos \alpha^* + d_3^{(ij)} = 0, \quad (28)$$

where $d_1^{(ij)}, d_2^{(ij)}, d_3^{(ij)}$ are coefficients computed from correspondences. As a result, the consensus maximization problem can be formulated as follows

$$\begin{aligned} \max_{\alpha, \mathcal{I}} & |\mathcal{I}| \\ \text{s.t.} & |d(\alpha)^{(ij)}| \leq \epsilon, \\ & \forall ((\mathbf{p}_i, \mathbf{u}_i), (\mathbf{p}_j, \mathbf{u}_j)) \in \mathcal{I}. \end{aligned} \quad (29)$$

Plain BnB [27]. Denote the lower bound of $|d(\alpha)^{(ij)}|$ on a subcube $\mathcal{C}_{\text{plain}}$ as $L(\mathcal{C}_{\text{plain}})$ and the upper bound as

$U(\mathcal{C}_{plain})$. $L(\mathcal{C}_{plain})$ can be simply computed by the centre point of the cube. On the cube \mathcal{C}_{plain} , we can obtain $d_l^{(ij)} \leq d(\alpha)^{(ij)} \leq d_r^{(ij)}$, thus the upper bound can be derived from the observation

$$\begin{aligned} \max_{\alpha} \sum_{ij} \mathbf{1}(|d(\alpha)^{(ij)}| \leq \epsilon) &= \max_{\alpha} \sum_{ij} \mathbf{1}(-\epsilon \leq d(\alpha)^{(ij)} \leq \epsilon) \\ &\leq \sum_{ij} \mathbf{1}(d_l^{(ij)} \leq \epsilon \text{ and } -\epsilon \leq d_r^{(ij)}) \\ &=: U(\mathcal{C}_{plain}), \end{aligned} \quad (30)$$

where $\mathbf{1}(\cdot)$ is the indicator function.

ACM-0: Interval Stabbing. Given that ACM can be used to replace n -dimensional plain BnB by branching over an $(n-1)$ -dimensional space, only, we name our proposed solutions for specific n -dimensional problems as ACM- $(n-1)$. For example, in the case of the presently solved 1-dimensional CM problem, the method is denoted ACM-0. For an inequality $|d_1^{(ij)} \sin \alpha + d_2^{(ij)} \cos \alpha + d_3^{(ij)}| < \epsilon$ that is composed of basic functions like *sine* and *cosine*, we can inversely solve for the interval of α with the assumption that $\alpha \in [-\pi, \pi]$. See the appendix for more details about the angular interval resulting from constraints like (28). Each data pair $((\mathbf{p}_i, \mathbf{u}_i), (\mathbf{p}_j, \mathbf{u}_j))$ then leads to an interval for α denoted $[\alpha_{ij}^l, \alpha_{ij}^r]$. Hence, interval stabbing can be used to directly solve for the optimal α without BnB as follows

$$\begin{aligned} \max_{\alpha} \sum_{ij} \mathbf{1}(|d(\mathcal{C}_{ACM})^{ij}| \cap [0, \epsilon]) \\ = \max_{\alpha} \sum_{ij} \mathbf{1}(\alpha \in [\alpha_{ij}^l, \alpha_{ij}^r]). \end{aligned} \quad (31)$$

5.1 Synthetic Experiments

Setup. We present the following synthetic experiments to verify the advantage of ACM-0 over 1-dimensional plain BnB. To generate synthetic image correspondences, we randomly sample 200 3D points in the cube $[-1, 1]^2 \times [4, 8]$, and then generate the correspondences from rays that point to the same 3D point. To add noise, we first extract an orthogonal plane from each bearing vector and add random noise in pixels by assuming a focal length of 800 for the orthogonal plane. The perturbed points in the plane are renormalized to obtain perturbed bearing vectors [5].

Elements of translation \mathbf{t} and the rotation angles are randomly generated in the interval $[-1, 1]$ and $[-\pi/2, \pi/2]$, respectively. We furthermore add randomly sampled noise from $[-2, 2]$ pixels for the image points, set 0.2 as the inlier threshold for the algebraic constraint in (29), and adopt 10 as the maximal depth for plain BnB. All algorithms are implemented in C++ and repeated 100 times on different random data to gain stable results. The angular error is measured as $|\alpha_{gt} - \alpha_{hat}|$ in degrees, where α_{gt} and α_{hat} are the ground truth and the estimated angle, respectively.

Results. As discussed previously, while plain BnB iteratively branches over intervals in 1 dimension, ACM-0 just directly uses Interval Stabbing, hence the problem (29) can be solved much more efficiently. In the following, we investigate the running time of plain BnB and ACM-0 and validate the performance of Interval Stabbing. Fig. 5a shows the mean results of plain BnB and ACM-0 where we vary the

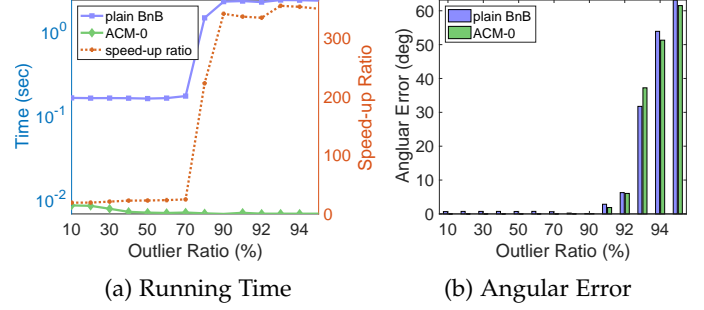


Fig. 5: 3D-2D registration experiments (Section 5) where we compare ACM-0 and the plain BnB method of [27]. ACM-0 is more than 200 times faster in the high-outlier regime (Fig. 5a) with comparable angular errors (Fig. 5b). (200 randomly generated noisy correspondences, 100 trials)

TABLE 1: Number of iterations of plain BnB [27], which is always 1 for ACM-0.

ratio	80%	90%	91%	92%	93%	94%	95%
iter	1,138	1,842	1,861	1,822	1,920	1,898	1,899

outlier ratio from 10% to 90% with a stepsize of 10%, and from 91% to 95% with a stepsize of 1%. TABLE 1 presents the average number of iterations of plain BnB in large outlier ratio conditions.

In general, ACM-0 is consistently faster than plain BnB and enjoys a $200 \times$ – $300 \times$ speed-up ratio while leading to similar angular errors. More importantly, ACM-0 solves the 1-dimensional problem globally optimally in real-time, while plain BnB does not attain real-time capabilities. More specifically, ACM-0 converges after about 10^{-2} sec even in extreme outlier cases (outlier ratio above 80%), while plain BnB needs over 1 sec and more than 10^3 iterations to complete. As furthermore shown in Fig. 5b, we obtain consistent angular errors with the method of Jiao et al. [27].

6 ACM-1: 2D-2D REGISTRATION

Next, we consider a 2-dimensional Consensus Maximization problem and demonstrate how ACM can again achieve considerable acceleration by branching over a 1-dimensional search space, only. We consider the case of a forward-looking camera installed on a planar ground vehicle (e.g. a car driving on a flat road). The motion of the camera will be constrained to a plane, hence frame-to-frame visual odometry can be solved by finding a 3-dimensional Euclidean transformation composed of a 2-dimensional translational and a 1-dimensional rotational displacement in the plane. Note that this stands in contrast with five degrees of freedom in the general, calibrated relative pose scenario. By using an angle-plus-parallax parametrization and substituting in the epipolar constraint, the unobservable parallax is easily eliminated thereby resulting in a two-angle problem that can be solved globally optimally using plain BnB [26].

Problem formulation. Consider a pair of 2D-2D correspondences $(\mathbf{x}_i, \mathbf{x}'_i)$ originating from the forward-looking camera on the vehicle under planar motion as illustrated in Fig. 6,

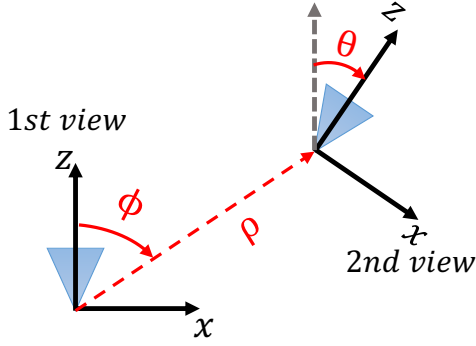


Fig. 6: Visualization of the planar motion. The rotation is parametrized by an angle θ as shown in (34), and translation by its length ρ and angle ϕ as shown in (35).

where $\mathbf{x}_i = [u_1, v_1]^T \in \mathbb{R}^2$ and $\mathbf{x}'_i = [u_2, v_2]^T \in \mathbb{R}^2$ denote the normalized image coordinates from the 1st view and 2nd view respectively. The correspondences follow an underlying relative pose transformation constraint depending on $\mathbf{R}^* \in SO(3)$ and $\mathbf{t}^* \in \mathbb{R}^3$. It is given by

$$\mathbf{x}_i = \pi(\mathbf{R}^* \mathbf{x}'_i + \mathbf{t}^*) \quad (32)$$

where $\pi: \mathbb{R}^3 \rightarrow \mathbb{R}^2$ denotes the camera projection function. Then the epipolar constraint is given by

$$(\tilde{\mathbf{x}}_i)^T \mathbf{E}^* \tilde{\mathbf{x}}'_i = 0, \quad (33)$$

where $\tilde{\mathbf{x}}_i = [\mathbf{x}_i^T, 1]^T$, $\tilde{\mathbf{x}}'_i = [\mathbf{x}'_i^T, 1]^T$, and $\mathbf{E}^* = [\mathbf{t}^*]_{\times} \mathbf{R}^*$ is the essential matrix composed of camera rotation $\mathbf{R}^* \in SO(3)$ and translation $\mathbf{t}^* \in \mathbb{R}^3$ from the 2nd view to the 1st view.

Without loss of generality, we assume that the y -axis of the camera is pointing downwards and the principal axis forward. Given the planar motion of the vehicle in the horizontal plane, the rotation matrix \mathbf{R}^* from the 2nd view to 1st view is given by the single-angle parameter matrix

$$\mathbf{R}^* = \begin{bmatrix} \cos \theta^* & 0 & \sin \theta^* \\ 0 & 1 & 0 \\ -\sin \theta^* & 0 & \cos \theta^* \end{bmatrix}, \quad (34)$$

where θ^* is the yaw angle about the y axis. Denoting ρ^* the length of the translation vector and ϕ^* the direction angle of the translation with respect to the original position, the planar translation \mathbf{t}^* is given by

$$\mathbf{t}^* = \begin{bmatrix} \rho \sin \phi^* \\ 0 \\ \rho \cos \phi^* \end{bmatrix}. \quad (35)$$

See Fig. 6 for a visualization of this setup.

Substituting \mathbf{R}^* and \mathbf{t}^* into (33), we can easily obtain

$$\begin{aligned} u_1 v_2 \cos \phi^* - v_2 \sin \phi^* \\ - u_2 v_1 \cos(\theta^* - \phi^*) - v_1 \sin(\theta^* - \phi^*) = 0, \end{aligned} \quad (36)$$

where the length of the translation ρ^* has been eliminated and only the 2 unknown angles θ^* and ϕ^* are left to be found.

Reformulating (36) in order to separate the unknown parameters, we can get

$$A_1 \sin(\theta_1^* + \phi_1^*) + A_2 \sin(\theta_2^* + \phi_2^*) = 0, \quad (37)$$

where $\theta_1^* = \theta^* - \phi^*$, $\theta_2^* = \phi$ and A_1, A_2, ϕ_1 and ϕ_2 are coefficients computed from \mathbf{x}_1 and \mathbf{x}_2 . Denoting $g_i(\theta_1, \theta_2) = A_1^{(i)} \sin(\theta_1 + \phi_1^{(i)}) + A_2^{(i)} \sin(\theta_2 + \phi_2^{(i)})$ as the above constraint for each correspondence $i = 1, \dots, M$, the Consensus Maximization problem can be naturally formulated as follows:

$$\begin{aligned} \max_{\theta_1, \theta_2, \mathcal{I}} |\mathcal{I}| \\ \text{s.t. } |g_i(\theta_1, \theta_2)| \leq \epsilon, \forall (\mathbf{x}_i, \mathbf{x}'_i) \in \mathcal{I}. \end{aligned} \quad (38)$$

Plain BnB [26]. Note that the bounds generally described in Section 3 can be used to bound $|g_i(\theta_1, \theta_2)|$. Given a sub-cube $\mathcal{C}_{\text{plain}}$ with the centre point $[\theta_1^c, \theta_2^c]$ and $g_i^l \leq g_i(\mathcal{C}_{\text{plain}}) \leq g_i^r$, the lower bound $L(\mathcal{C}_{\text{plain}})$ and the upper bound $U(\mathcal{C}_{\text{plain}})$ are given by

$$L(\mathcal{C}_{\text{plain}}) = \sum_i \mathbf{1}(|g_i(\theta_1^c, \theta_2^c)| \leq \epsilon) \quad (39)$$

$$U(\mathcal{C}_{\text{plain}}) = \sum_i \mathbf{1}(g_i^l \leq \epsilon \text{ and } g_i^r \geq -\epsilon). \quad (40)$$

ACM-1. Without loss of generality, suppose ACM-1 is used to branch over the space of θ_1 , and θ_2 is searched by Interval Stabbing. First, consider the lower bound estimated by ACM-1. As mentioned for plain BnB, a trivial lower bound on a subcube $\mathcal{C}_{\text{plain}}$ can be obtained by the centre point $[\theta_1^c, \theta_2^c]$. Denoting the interval of θ_2 inversely derived from $g_i(\theta_1^c, \theta_2)$ as $[\theta_{2i}^l, \theta_{2i}^r]$ (See the appendix for details), the lower bound for ACM-1 on a subcube \mathcal{C}_{ACM} can be obtained by solving the Interval Stabbing problem

$$\begin{aligned} L(\mathcal{C}_{\text{ACM}-1}) &= \max_{\theta_2} \sum_i \mathbf{1}(|g_i(\theta_1^c, \theta_2)| \leq \epsilon) \\ &= \max_{\theta_2} \sum_i \mathbf{1}(\theta_2 \in [\theta_{2i}^l, \theta_{2i}^r]). \end{aligned} \quad (41)$$

As introduced in Section 4, the upper bound of ACM-1 can be obtained by solving the Interval Stabbing problem

$$\begin{aligned} U(\mathcal{C}_{\text{ACM}-1}) &= \max_{\theta_2} \sum_i \mathbf{1}(|g_i(\mathcal{C}_{\text{ACM}-1}, \theta_2)| \cap [0, \epsilon]) \\ &= \max_{\theta_2} \sum_i \mathbf{1}(\theta_2 \in [\bar{\theta}_{2i}^l, \bar{\theta}_{2i}^r]). \end{aligned} \quad (42)$$

6.1 Synthetic Experiments

Setup. We use the same setting with noise as mentioned in the last section except that now the camera undergoes planar rotation and translation to generate coordinates in a second view. We randomly sample the yaw angle within the interval $[-\pi/3, \pi/3]$ while the roll and pitch angles are kept to 0. The translation angle is sampled from the interval $[-\pi/3, \pi/3]$, and the translation norm ρ from the interval $[-2, 2]$. We still use 10 as the maximal depth and 0.02 as the inlier threshold for both plain BnB [26] and ACM-1.

Results. We implement both plain BnB [26] and ACM-1 based on the bounding functions defined previously and investigate their relative performance. We were not able to run the code of [26], so we implemented our own version of plain BnB. In [26] it was written that their implementation took 18 seconds to process 50 correspondences from two consecutive KITTI images with 10^{-4} inlier threshold. On the other hand, our implementation took fewer than 1 second to process 200 SIFT correspondences with the same inlier

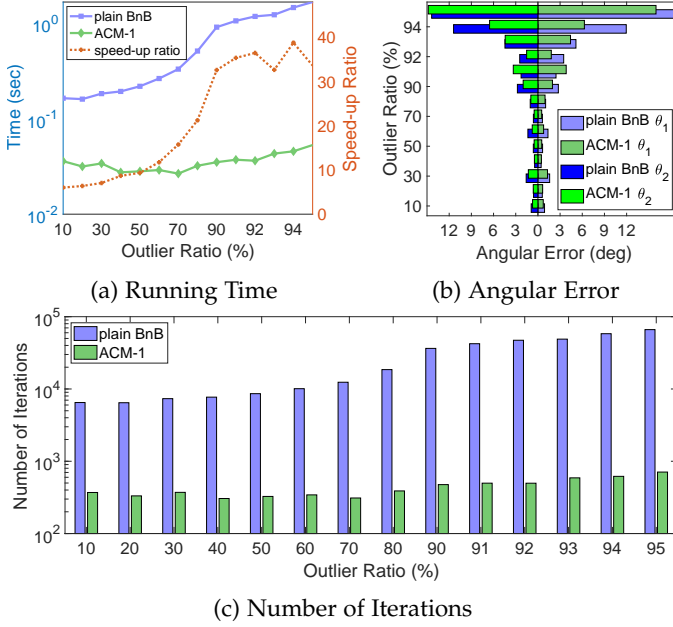


Fig. 7: 2D-2D registration experiments (Section 6.1). ACM-1 attains $20\times$ speed-up over plain BnB at extreme outlier rates (Fig. 7a) with comparable angular errors (Fig. 7b) and converging within much fewer iterations (Fig. 7c). (200 randomly generated noisy correspondences, 100 trials)

threshold 10^{-4} . This validates the correctness and efficiency of our implementation of plain BnB as a baseline.

The outlier ratio is varied from 10% to 90% with a step size of 10%, and then from 91% to 95% with a step size of 1%. The mean results are displayed in Fig. 7. As expected, it is clear that ACM-2 needs much less time to converge than plain BnB and achieves a $2\times\text{--}20\times$ speed-up ratio (Fig. 7a). At the same time, ACM-2 maintains similarly low angular errors than plain BnB for both θ_1 and θ_2 (Fig. 7b). Taking a detailed look at Fig. 7a indicating run-times, ACM-2 stably takes an average of about 0.03s for a wide range of outlier ratios. This is contrast to plain BnB, for which running times are much more sensitive with respect to the outlier ratio and increase from 0.0615s to 0.5833s. Taking into account the significant difference in the number of iterations as shown in Fig. 7c, this result also confirms our claim that in practice the extra $\log M$ complexity for interval stabbing in each iteration is negligible.

6.2 Real Experiments

In order to verify the effectiveness of our algorithm for globally optimal 2D-2D registration, we conducted real-world experiments using the KITTI dataset [50].

Setup. We process all 11 sequences (00-10) containing ground truth. We extract SIFT features [51] for each image, set the number of best features to retain (n_{features}) to 1000, and perform brute-force matching of feature points on pairs of consecutive frames. Finally, the obtained pixel correspondences were normalized using the known intrinsic camera matrix. Ground truth relative pose parameters \mathbf{R} and \mathbf{t} are extracted by concatenating the corresponding absolute poses, followed by extraction of the ground truth values for θ_{gt} and ϕ_{gt} .

The threshold ϵ for the algebraic error is set to 10^{-4} , and the maximal depth for plain BnB and ACM-1 are set to 20 to obtain more precise solutions. The initial cubes of plain BnB and ACM-1 are defined as $[-\pi/2, \pi/2]^2$ and $[-\pi/2, \pi/2]$ respectively. Errors are expressed by the absolute difference between estimated and ground truth angles θ and ϕ .

Results. Results on the KITTI datasets again demonstrate the expected speed-up of ACM-1 over plain BnB. The median results over all image pairs in each sequence are summarised in TABLE 2. Overall, ACM-1 obtains about a $2\times$ speed-up and almost identical errors. The faster running time of ACM-1 is again the result of a significantly reduced number of iterations. Note that—although the SIFT feature is rather old—it still returns high-quality correspondences between the pairs of views, thereby leading to low outlier scenarios in which the advantage of ACM over plain BnB is less pronounced.

7 ACM-2: 3D-3D REGISTRATION

In this section, we apply ACM to the problem of 3D point set registration (i.e. Procrustes alignment), which aims at aligning two point sets by a rigid transformation.

Problem formulation Consider two overlapping noiseless 3D point sets $\mathcal{P} = \{\mathbf{p}_i\}_{i=1}^{M_1}$ and $\mathcal{Q} = \{\mathbf{q}_j\}_{j=1}^{M_2}$. Each overlapping pair $(\mathbf{p}_i, \mathbf{q}_j)$ satisfies the relation

$$\mathbf{q}_j = \mathbf{R}^*(\mathbf{p}_i + \mathbf{t}^*), \quad (43)$$

where $\mathbf{R}^* \in SO(3)$ and $\mathbf{t}^* \in \mathbb{R}^3$ represent the underlying rotation and translation respectively. Instead of solving the 6-DoF problem directly, it has been shown that algebraic operations can be used to eliminate 3 DoF and solve globally for the resulting 3-DoF problem by Branch and Bound. Furthermore, ACM can reduce 1 more DoF to solve it by branching over a 2-dimensional search space.

Similar to the problem of image registration, it is possible to extract 3D features on point sets and match correspondences, which leads to correspondence-based 3D-3D registration. On the other hand, it is also possible to simultaneously search for transformation and correspondence, thereby leading to so-called correspondence-less registration. In the following, we present ACM-2 for both variants of 3D point set registration. We name ACM for the correspondence-based 3D-3D registration problem *ACM-2 Corr*, and ACM for correspondence-less 3D-3D registration *ACM-2 Corrless*.

7.1 Correspondence-based Registration

Provided a set of 3D point correspondences $\{(\mathbf{p}_i, \mathbf{q}_i)\}_{i=1}^M$, where $\mathbf{p}_i, \mathbf{q}_i \in \mathbb{R}^3$, the problem of correspondence-based point set registration can be understood as finding the rotation \mathbf{R}^* and translation \mathbf{t}^* that satisfy the relation

$$\mathbf{q}_i = \mathbf{R}^*(\mathbf{p}_i + \mathbf{t}^*), \quad (44)$$

where we omitted noise for simplicity. Taking the norm on both sides, rotation invariance easily leads to the constraint

$$\|\mathbf{q}_i\|_2 = \|\mathbf{p}_i + \mathbf{t}^*\|_2. \quad (45)$$

TABLE 2: Experiments on the KITTI dataset (Section 6.2). Results are the median over all image pairs of each sequence.

Metric	Method \ Seq.	00	01	02	03	04	05	06	07	08	09	10
Rot (deg)	plain BnB	0.1304	0.1052	0.0894	0.1053	0.0544	0.0730	0.0862	0.0635	0.0765	0.0802	0.0879
	ACM-1	0.1293	0.1050	0.0891	0.1008	0.0536	0.0733	0.0872	0.0622	0.0767	0.0801	0.0852
Trans (deg)	plain BnB	4.4905	2.6027	2.6733	5.2189	1.3994	3.5529	2.9525	4.7887	3.2316	2.9904	3.2244
	ACM-1	4.4743	2.5903	2.6752	5.4160	1.4357	3.5397	2.9182	4.7979	3.2276	2.9550	3.1836
Time (sec)	plain BnB	1.0639	0.5721	0.9455	1.7012	0.8860	1.1202	0.8915	1.4539	1.0266	0.9447	1.0122
	ACM-1	0.5041	0.3033	0.4697	0.7798	0.5364	0.5390	0.4561	0.7330	0.5158	0.4786	0.4871
Iter	plain BnB	16,234	10,047	15,571	22,793	13,524	16,238	14,043	19,926	16,107	15,198	15,951
	ACM-1	1,692	1,307	1,712	2,197	1,713	1,750	1,664	2,095	1,792	1,711	1,714
Speed Up Ratio		2.0116	1.8783	1.9562	2.1045	1.5778	1.9840	1.9061	1.9645	1.8939	1.9430	1.9971

The unknown rotation \mathbf{R}^* is thus eliminated, and the unknown translation \mathbf{t}^* can be solved by the following Consensus Maximization problem

$$\begin{aligned} \max_{\mathbf{t}, \mathcal{I}} |\mathcal{I}| \\ \text{s.t. } \|\mathbf{q}_i\|_2 - \|\mathbf{p}_i + \mathbf{t}\|_2 \leq \epsilon, \forall (\mathbf{p}_i, \mathbf{q}_i) \in \mathcal{I} \end{aligned} \quad (46)$$

Plain BnB. Let us define $h_i(\mathbf{t}) = \|\mathbf{q}_i\|_2 - \|\mathbf{p}_i + \mathbf{t}\|_2$. Given a subcube $\mathcal{C}_{\text{plain}}$ with the centre point \mathbf{t}_c , we may denote the interval of $h_i(\mathbf{t})$ on this volume as $[h_i^l, h_i^r]$. Again, a trivial lower bound and the intuitive upper bound result to

$$L(\mathcal{C}_{\text{plain}}) = \sum_i \mathbf{1}(h_i(\mathbf{t}_c) \leq \epsilon) \quad (47)$$

$$U(\mathcal{C}_{\text{plain}}) = \sum_i \mathbf{1}(h_i^l \leq \epsilon \text{ and } h_i^r \geq -\epsilon). \quad (48)$$

ACM-2 Corr. Write the translation \mathbf{t} and point \mathbf{p}_i respectively as $\mathbf{t} = [t_1, t_2, t_3]^T$ and $\mathbf{p}_i = [p_{1i}, p_{2i}, p_{3i}]^T$. Without loss of generality, let ACM-2 branch over the first two dimensions of the translation space and solve globally optimally for t_3 using Interval Stabbing.

For the constraint $h_i(\mathbf{t}) \leq \epsilon$, we can derive

$$-\epsilon \leq \|\mathbf{q}_i\|_2 - \|\mathbf{p}_i + \mathbf{t}\|_2 \leq \epsilon \quad (49)$$

$$\Leftrightarrow \|\mathbf{q}_i\|_2 - \epsilon \leq \|\mathbf{p}_i + \mathbf{t}\|_2 \leq \|\mathbf{q}_i\|_2 + \epsilon \quad (50)$$

$$\Leftrightarrow (\|\mathbf{q}_i\|_2 - \epsilon)^2 \leq \|\mathbf{p}_i + \mathbf{t}\|_2^2 \leq (\|\mathbf{q}_i\|_2 + \epsilon)^2. \quad (51)$$

Since $\|\mathbf{p}_i + \mathbf{t}\|_2^2$ can be separated into two additive parts, $h_1(t_1, t_2) = (p_{1i} + t_1)^2 + (p_{2i} + t_2)^2$ and $h_2(t_3) = (p_{3i} + t_3)^2$, this is a special case of Example 1. In particular, according to Section 4.1, the lower bound for ACM-1 here arises as

$$\begin{aligned} L(\mathcal{C}_{\text{ACM}}) &= \max_{t_3} \sum_i \mathbf{1}(|h_i(t_1^c, t_2^c; t_3)| \leq \epsilon) \\ &= \max_{t_3} \sum_i \mathbf{1}(t_3 \in [\underline{t}_{3i}^l, \underline{t}_{3i}^r]), \end{aligned} \quad (52)$$

and the upper bound of ACM-1, can be derived similarly follows from Example 1 (see also the appendix for details):

$$\begin{aligned} U(\mathcal{C}_{\text{ACM}}) &= \max_{t_3} \sum_i \mathbf{1}(|h_i(\mathcal{C}_{\text{ACM}}; t_3)| \leq \epsilon) \\ &= \max_{t_3} \sum_i \mathbf{1}(t_3 \in [\bar{t}_{3i}^l, \bar{t}_{3i}^r]). \end{aligned} \quad (53)$$

7.2 Correspondence-less Registration

Limited by the quality and distinctiveness of point cloud feature descriptors, matching correspondences can be problematic. This has motivated researchers to design

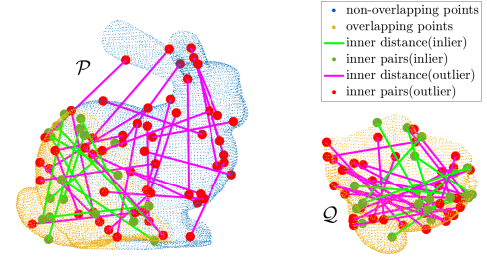


Fig. 8: Visualization of the correspondence-less registration setup (Section 7.2) and the Bunny experiment (Section 7.4). The full Bunny point set on the left can be regarded as the reference set. The partial Bunny point cloud on the right is the moving set and constitutes the overlapping part after a motion compensation. The length of the inter-pair line segments is invariant when point sets rigidly move.

correspondence-less methods. For example, registration with all-to-all matching lists is considered in [34]. Using the key observation that inner distances of a point set are invariant with respect to rigid transformations (cf. Fig. 8), Liu et al. [32] furthermore propose to filter out most of the useless correspondences and then feed them to a plain BnB called GoTS to search the translation and correspondences simultaneously.

Formally, using the general problem formulation in (43), suppose the point pairs $(\mathbf{q}_{i1^*}, \mathbf{q}_{i2^*})$ are randomly picked from the overlapping point part of set \mathcal{Q} and the pairs $(\mathbf{p}_{j1^*}, \mathbf{p}_{j2^*})$ are the corresponding ground truth pairs from the reference point set \mathcal{P} . One key observation is that

$$\begin{aligned} \|\mathbf{q}_{i1^*} - \mathbf{q}_{i2^*}\|_2 &= \|\mathbf{R}(\mathbf{p}_{j1^*} + \mathbf{t}) - \mathbf{R}(\mathbf{p}_{j2^*} + \mathbf{t})\|_2 \\ &= \|\mathbf{p}_{j1^*} - \mathbf{p}_{j2^*}\|_2, \end{aligned} \quad (54)$$

where $\mathbf{R} \in SO(3)$ is any rotation matrix and $\mathbf{t} \in \mathbb{R}^3$ is any translation. Note that for ground truth pairs $(\mathbf{q}_{i1^*}, \mathbf{q}_{i2^*})$ and $(\mathbf{p}_{j1^*}, \mathbf{p}_{j2^*})$, the distance $|\|\mathbf{q}_{i1^*} - \mathbf{q}_{i2^*}\|_2 - \|\mathbf{p}_{j1^*} - \mathbf{p}_{j2^*}\|_2|$ is expected to be small, therefore, with an appropriate threshold τ , we can then keep only the pair $((\mathbf{q}_{i1}, \mathbf{q}_{i2}), (\mathbf{p}_{j1}, \mathbf{p}_{j2}))$ that satisfies

$$|\|\mathbf{q}_{i1} - \mathbf{q}_{i2}\|_2 - \|\mathbf{p}_{j1} - \mathbf{p}_{j2}\|_2| \leq \tau, \quad (55)$$

for every $i1, i2 \in \{1, \dots, M_1\}$ and every $j1, j2 \in \{1, \dots, M_2\}$ ($i1 \neq i2, j1 \neq j2$), and remove all other pairs. The remaining point pairs $((\mathbf{q}_{i1}, \mathbf{q}_{i2}), (\mathbf{p}_{j1}, \mathbf{p}_{j2}))$ are called Rotation Invariant (RI) pairs.

Next, observe that $\|\mathbf{q}_i\| = \|\mathbf{p}_j + \mathbf{t}^*\|$ further provides constraints for RI pairs. Using the ℓ_∞ norm, we have

$$\|\mathbf{F}_{m,n}(\mathbf{t}^*)\|_\infty \leq \epsilon, \quad (56)$$

$$\mathbf{F}_{m,n}(\mathbf{t}) := \begin{bmatrix} \|\mathbf{p}_{i1} + \mathbf{t}\|_2 - \|\mathbf{q}_{j1}\|_2 \\ \|\mathbf{p}_{i2} + \mathbf{t}\|_2 - \|\mathbf{q}_{j2}\|_2 \end{bmatrix}, \quad (57)$$

where $m := (i1, i2), n := (j1, j2)$. We can then formulate the Consensus Maximization problem as:

$$\begin{aligned} \max_{\mathbf{t}, \mathcal{I}} \quad & |\mathcal{I}| \\ \text{s.t.} \quad & \|\mathbf{F}_{m,n}(\mathbf{t})\|_\infty \leq \epsilon, \\ & \forall ((\mathbf{p}_{j1}, \mathbf{p}_{j2}), (\mathbf{q}_{i1}, \mathbf{q}_{i2})) \in \mathcal{I}. \end{aligned} \quad (58)$$

Note that the constraint $\|\mathbf{F}_{m,n}(\mathbf{t})\|_\infty \leq \epsilon$ —which aims to check whether the largest element between $\|\mathbf{p}_{i1} + \mathbf{t}\|_2 - \|\mathbf{q}_{j1}\|_2$ and $\|\mathbf{p}_{i2} + \mathbf{t}\|_2 - \|\mathbf{q}_{j2}\|_2$ is smaller than ϵ —can also be interpreted as a check whether $\|\mathbf{p}_{i1} + \mathbf{t}\|_2 - \|\mathbf{q}_{j1}\|_2 \leq \epsilon$ and $\|\mathbf{p}_{i2} + \mathbf{t}\|_2 - \|\mathbf{q}_{j2}\|_2 \leq \epsilon$ at the same time.

Remark 2. The problem formulated in (58) is not exactly the same as the one in [32], where they solve

$$\max_{\mathbf{t}} \sum_m \max_n \mathbf{1}(\|\mathbf{F}_{m,n}(\mathbf{t})\|_\infty \leq \epsilon). \quad (59)$$

Note that the main difference between (58) and (59) is the number of counted inliers. As can be observed, (59) seeks a unique correspondence for each m . It is easy to prove though that the solution of (58) is also the solution of (59) (see the appendix).

Plain BnB. Given the cube \mathcal{C}_{plain} with centre point \mathbf{t}_c and half of its diameter r_{plain} , the lower bound is again trivially given by using \mathbf{t}_c . To provide a clear explanation on the upper bound, let us use the new index notation $u := (i1, j1), v := (i2, j2)$. For any translation \mathbf{t} of the cube \mathcal{C}_{plain} and $\mathbf{x} \in \mathbb{R}^3$, we have a basic geometric inequality

$$\|\mathbf{x} + \mathbf{t}_c\|_2 - r_{plain} \leq \|\mathbf{x} + \mathbf{t}\|_2 \leq \|\mathbf{x} + \mathbf{t}_c\|_2 + r_{plain}. \quad (60)$$

Therefore, for each pair $(\mathbf{p}_{i1}, \mathbf{q}_{j1})$, writing $c_u := \|\mathbf{q}_{j1}\|_2 - \|\mathbf{p}_{i1} + \mathbf{t}_c\|_2$, we can get

$$c_u - r_{plain} \leq \|\mathbf{q}_{j1}\|_2 - \|\mathbf{p}_{i1} + \mathbf{t}\|_2 \leq c_u + r_{plain}, \quad (61)$$

$$c_u^l \leq \|\mathbf{q}_{j1}\|_2 - \|\mathbf{p}_{i1} + \mathbf{t}\|_2 \leq c_u^r, \quad (62)$$

where $c_u^l = \min\{0, |c_u - r_{plain}|, |c_u + r_{plain}|\}$ and $c_u^r = \max\{|c_u - r_{plain}|, |c_u + r_{plain}|\}$. Similarly, denote $c_v = \|\mathbf{q}_{j2}\|_2 - \|\mathbf{p}_{i2} + \mathbf{t}_c\|_2$, $c_v^l = \min\{0, |c_v - r_{plain}|, |c_v + r_{plain}|\}$ and $c_v^r = \max\{|c_v - r_{plain}|, |c_v + r_{plain}|\}$. We now can obtain

$$\begin{aligned} \|\mathbf{F}_{m,n}(\mathcal{C}_{plain})\|_\infty &= \max\{[c_u^l, c_u^r], [c_v^l, c_v^r]\} \\ &= [\max\{c_u^l, c_v^l\}, \max\{c_u^r, c_v^r\}]. \end{aligned} \quad (63)$$

Therefore, the upper bound of plain BnB is defined by

$$\begin{aligned} U(\mathcal{C}_{plain}) &= \sum_{u,v} \mathbf{1}([\max\{c_u^l, c_v^l\}, \max\{c_u^r, c_v^r\}] \cap [0, \epsilon]) \\ &= \sum_{u,v} \mathbf{1}(\max\{c_u^l, c_v^l\} \leq \epsilon) \\ &\geq \max_{\mathbf{t}} \sum_{u,v} \mathbf{1}(\|\mathbf{F}_{u,v}(\mathbf{t})\|_\infty \leq \epsilon). \end{aligned} \quad (64)$$

ACM-2 Corrless. Without the loss of generality, suppose ACM-2 Corrless branches over the first two dimensions, and

uses Interval Stabbing to find t_3 . Given the cube \mathcal{C}_{ACM} with centre point $\mathbf{t}_{c(1:2)}$ and its half-diameter r_{ACM} , consider the following sub-constraint for each pair $(\mathbf{p}_{i1}, \mathbf{q}_{j1})$

$$\|\mathbf{p}_{i1} + \mathbf{t}\|_2 - \|\mathbf{q}_{j1}\|_2 \leq \epsilon \quad (65)$$

$$\Leftrightarrow \|\mathbf{p}_{i1} + \mathbf{t}\|_2^2 \cap [(-\epsilon + \|\mathbf{q}_{j1}\|_2)^2, (\epsilon + \|\mathbf{q}_{j1}\|_2)^2]. \quad (66)$$

In order to separate out t_3 , let us define

$$h_1(\mathbf{p}_{i1(1:2)}, \mathbf{t}_{(1:2)}) = \|\mathbf{p}_{i1(1:2)} + \mathbf{t}_{(1:2)}\|_2^2 \quad (67)$$

$$h_2(\mathbf{p}_{i1(3)}, t_3) = \|\mathbf{p}_{i1(3)} + t_3\|_2^2, \quad (68)$$

such that $\|\mathbf{p}_{i1} + \mathbf{t}\|_2^2 = h_1(\mathbf{p}_{i1(1:2)}, \mathbf{t}_{(1:2)}) + h_2(\mathbf{p}_{i1(3)}, t_3)$.

Again, the lower bound of ACM-2 Corrless is modified from its pendant in plain BnB. Given $\mathbf{t}_{c(1:2)}$ and substituting $h_1(\mathbf{p}_{i1(1:2)}, \mathbf{t}_{c(1:2)})$ into (66), an interval $[t_{3u}^l, t_{3u}^r]$ for t_3 is again easily found by function inversion. Similarly, on the same cube we can derive another interval $[t_{3v}^l, t_{3v}^r]$ for t_3 from the sub-constraint on $(\mathbf{p}_{i2}, \mathbf{q}_{j2})$. Therefore, the trivial lower bound of ACM-2 Corrless is given by

$$L(\mathcal{C}_{ACM}) = \max_{t_3} \sum_{u,v} \mathbf{1}(t_3 \in [t_{3u}^l, t_{3u}^r] \cup [t_{3v}^l, t_{3v}^r]), \quad (69)$$

which can be solved globally by Interval Stabbing.

The upper bound of ACM-2 Corrless is derived in the same manner as in Example 1. Note that we can also get the 2-dimensional version of (60), denote the interval of $h_1(\mathbf{p}_{i1(1:2)}, \mathbf{t}_{(1:2)})$ on \mathcal{C}_{ACM} as

$$h_{1u}^l \leq h_1(\mathcal{C}_{ACM}, \mathbf{t}_{(1:2)}) \leq h_{1u}^r. \quad (70)$$

Relaxation on sub-constraint (66) is achieved by counting the following intervals

$$\begin{aligned} &h_2(\mathbf{p}_{i1(3)}, t_3) \\ &\in [(-\epsilon + \|\mathbf{q}_{j1}\|_2)^2 - h_{1u}^r, (\epsilon + \|\mathbf{q}_{j1}\|_2)^2 - h_{1u}^l] \\ &\Rightarrow t_3 \in [t_{3u}^l, t_{3u}^r]. \end{aligned} \quad (71)$$

Similarly, we can also derive the relaxed interval of t_3 on $(\mathbf{p}_{i2}, \mathbf{q}_{j2})$ and denote it as $[t_{3v}^l, t_{3v}^r]$. Finally, a valid upper bound of ACM-2 Corrless can be found by doing Interval Stabbing on the problem

$$U(\mathcal{C}_{ACM}) = \max_{t_3} \mathbf{1}(t_3 \in [t_{3u}^l, t_{3u}^r] \cup [t_{3v}^l, t_{3v}^r]). \quad (72)$$

Once the optimal translation \mathbf{t}^* is found, the unknown rotation \mathbf{R}^* can be efficiently estimated by existing rotation algorithms. For example, [31] proposed a 3-dimensional plain BnB with fast search, and [36] proposed an efficient and accurate method to simultaneously search rotation and correspondences.

7.3 Synthetic Experiments

Setup. The synthetic data generation for 3D-3D registration is similar to that in Section 5.1, except that we do not transform them into 2D features here. To introduce outliers, we randomly generate 3D points within the same range, transform them into one of the coordinate systems, and use them to replace the original inlier points. The relative translation and rotation axis are randomly generated in the unit cube. The rotation angle is randomly sampled in the interval $[-\pi, \pi]$. For correspondence-based registration, we first generate 3D-3D correspondences and then add noise

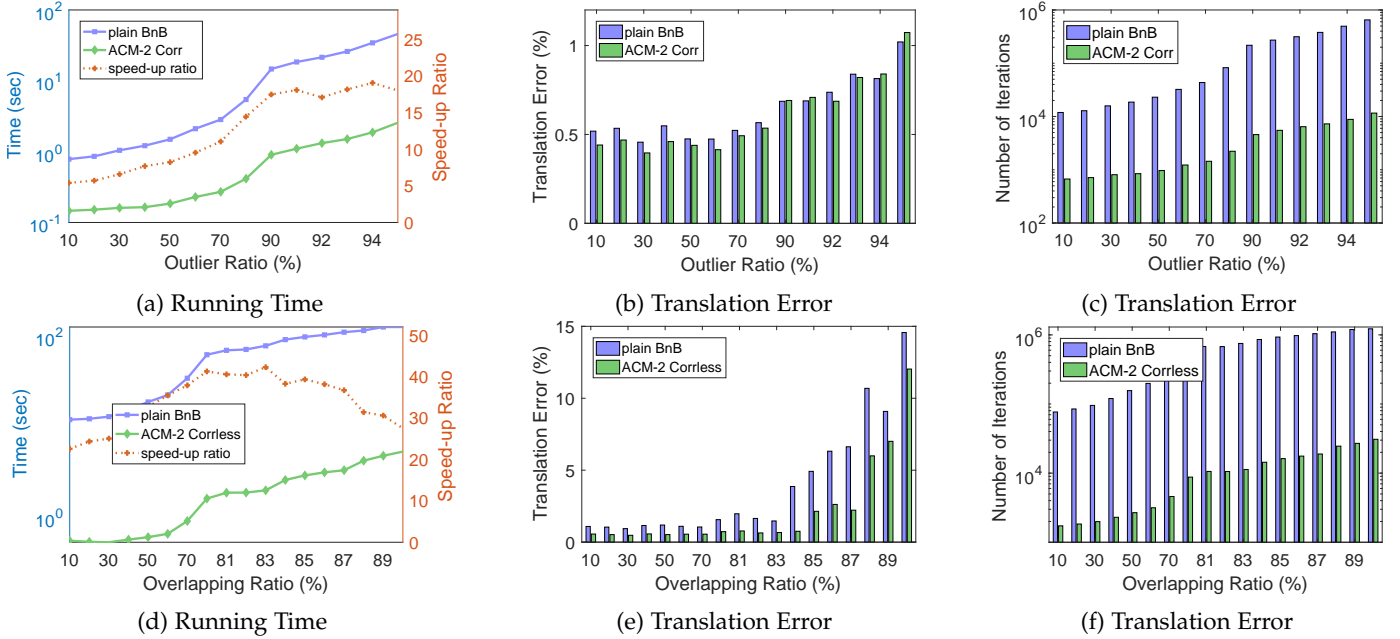


Fig. 9: 3D-3D registration experiments (Section 7.3). The first row shows the correspondence-less setting (Section 7.1) and the second row shows the correspondence-based setting (Section 7.2). ACM-2 Corr is 20× faster than plain BnB in the high-outlier regime (Fig. 9a) with comparable translation errors (Fig. 9b) and converging within much fewer iterations (Fig. 9c). Similar results are shown in Fig. 9d-Fig. 9f for the correspondence-less setting, where ACM-2 Corrless attains 30× - 40× speed-up. (1000 randomly generated correspondences, 100 trials)

from a Gaussian distribution with zero mean and 0.01 variance to the 3D points in both coordinate systems. For correspondence-less registration, we generate two noiseless point sets of the same size.

In both settings, we set the threshold $\epsilon = 0.001$ and matching threshold for correspondence-based setting $\tau = 0.1\epsilon$, the number of correspondences/points in each set to 1000, and we run 100 trials to get stable results. The maximal depth of plain BnB and ACM-2 Corr is set to 10. As suggested in [32], we keep 1000 point pairs with the largest inter-point distance in each point set for practical implementation in the correspondence-less setting. To measure translation errors, we define the relative translation error as $\frac{\|t_{hat} - t_{gt}\|_2}{\|t_{gt}\|_2}$, where t_{gt} is the ground truth translation and t_{hat} is the estimated translation.

Results. For the correspondence-based setting, the outlier ratio is varied from 10% to 90% in steps of 10%, and then from 91% to 95% in steps of 1%. The mean results are displayed in Fig. 9. For the correspondence-less setting, the overlapping ratio is varied from 10% to 70% in steps of 10%, and then from 81% to 90% in steps of 1%.

Considering Fig. 9a and 9d, it is obvious that significant improvements have been obtained in both settings. As can be observed, ACM-2 yields an order of magnitude faster results than plain BnB and the number of iterations of ACM-2 is about 2 orders of magnitude smaller than that of plain BnB. Similar errors are observed in all cases. When dealing with more extreme outlier ratios (larger than 90%) or extreme overlapping ratios (larger than 80%), ACM-2 Corr and ACM-2 Corrless are around 18× and 40× faster than plain BnB, respectively. These observations are in line with the previously discussed advantage of ACM that the

less 1-dimensional search space helps ACM to converge much faster.

7.4 Real Experiments

In our final experiment, we use the *bunny* point cloud from the Stanford 3D Scanning Repository [52] to compare ACM-2 Corrless and plain BnB.

Setup. We employ the *pcdownsample* [53] function from MATLAB to down-sample the original point cloud, which is in analogy with the setup used in [32]. To generate point sets, we then randomly cut the original bunny according to a certain overlap ratio and thereby obtain a fragment of the original point set. To conclude, we randomly transform this small fragment. The translation is randomly generated in $[-1, 1]^3$ and the rotation angles are randomly sampled from $[-\pi, \pi]$. Fig. 8 shows an example experiment setup with inliers and outliers as identified through the CM. To get RI pairs, we follow the same strategy as in [32]. We set the threshold to 10^{-4} and the maximal depth to 10. The initial cube of plain BnB is set to $[-1, 1]^3$ and $[-1, 1]^2$ for ACM-2 Corrless.

Results. Fig. 10 shows a comparison between plain BnB and ACM-2 Corrless, where we vary the overlap ratio from 10% to 90% (cf. first row), and then from 1% to 9% (cf. second row) to check extreme cases. ACM-2 Corrless presents a significant overall speed-up with respect to plain BnB while the translation errors remain comparable. To be specific, ACM-2 Corrless converges in less than 0.5 sec on average, whereas plain BnB needs more than 10 sec. The speed-up factor for ACM-2 Corrless therefore is about 40×. Interestingly, both methods can provide accurate estimation even in extreme cases where ACM-2 Corrless is more stable than plain BnB.

As can be identified in Fig. 10b, both methods can work in the majority of cases down to overlap ratios as low as 4%.

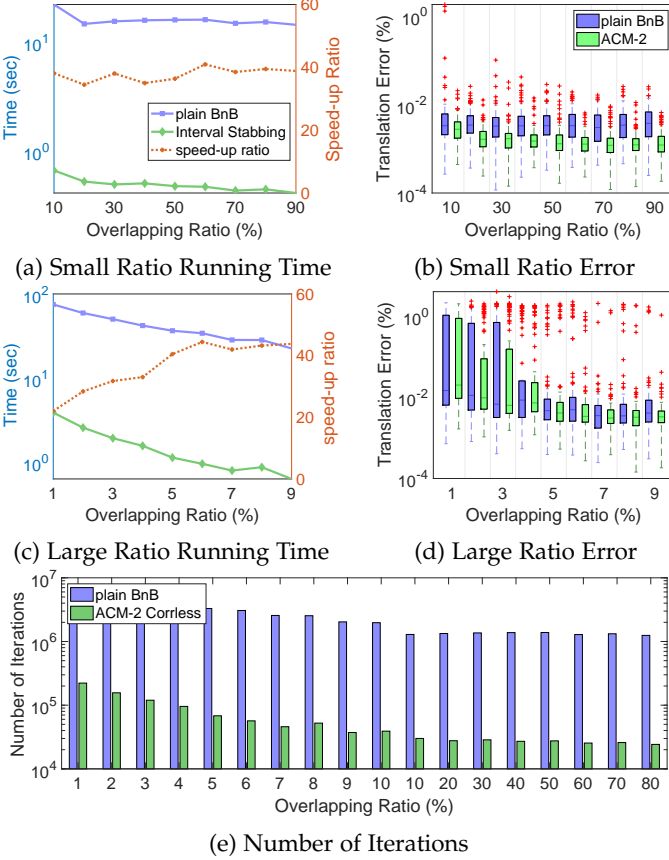


Fig. 10: 3D-3D correspondence-less registration experiments on Stanford Bunny (Section 7.4). ACM-2 Corr is $30 \times -40 \times$ faster than plain BnB (Fig. 10a 10c) with comparable translation errors (Fig. 10b 10d) and converging within much fewer iterations (Fig. 10e). (Mean results on 100 trials)

Remark 3. Note that the main contribution of this work is to an acceleration of consensus maximization, which we test on the noiseless, correspondence-less scenario addressed in [32]. Though this already serves well to highlight the advantages of our method, we nonetheless want to refer the reader to Zhang et al. [54] who introduce an extension of the approach to handle noise with the help of an initial state estimation.

8 CONCLUSION

In this work, we have introduced a general strategy to speed-up the solution of globally optimal consensus maximization via branch-and-bound. The proposed strategy consists of—for an n -dimensional problem—simply branching over an $(n-1)$ -dimensional space, and then solving for the remaining variable globally optimally using interval stabbing. Though the latter step takes on $\mathcal{O}(\log M)$ complexity, its cost is typically compensated for by the fact that much fewer volumes are created by branching over a smaller-dimensional space. Furthermore, embedding the globally optimal interval stabbing mechanism typically leads to tighter lower bounds, thereby causing earlier pruning of sub-optimal branches. We have validated our approach on

three fundamental geometric registration problems, including camera resectioning, relative camera pose estimation, and point set registration. In the latter case, we have even extended the application to the correspondence-less case by running the optimization over exhaustive match lists. This variant of the correspondence-less registration scenario is successfully solved owing to the algorithm’s strong ability to handle extreme outlier ratios. The attained execution times often hind at potential use in real-time applications, thereby lifting the relevance of globally optimal consensus maximization from a pure validation tool to a viable solution for online processing.

APPENDIX A PROOF OF PROPOSITION 1

Proof of Proposition 1. To count the number of iterations, we need to know how many times the initial cube is split.

- When $d = 1$, the initial cube is split into 2^n sub-cubes in the end.
- When $d = 2$, the initial cube is split into $2^n \cdot 2^n = (2^2)^n$ sub-cubes in the end.
- When $d = k$, the initial cube is split into $(2^k)^n = (2^k)^n$ sub-cubes in the end.

Perfect Bounds. Suppose BnB can keep the only sub-cube that contains the optimal solution after the bounding operation. Then the number of iterations for plain BnB is

$$1 + \underbrace{2^n + 2^n + \dots + 2^n}_d = \mathcal{O}(2^n), \quad (73)$$

and the number of iterations for ACM is

$$1 + \underbrace{2^{n-1} + 2^{n-1} + \dots + 2^{n-1}}_d = \mathcal{O}(2^{n-1}). \quad (74)$$

So in the case of perfect bounds, the number of iterations for ACM is about 2 times smaller than that of plain BnB.

Invalid Bounds. Suppose plain BnB and ACM do not prune any sub-cubes at each iteration, the number of iterations for plain BnB is as follows

$$1 + 2^n + (2^n)^2 + \dots + (2^n)^d = \mathcal{O}(2^{nd}), \quad (75)$$

and the number of iterations for ACM is

$$1 + 2^{n-1} + (2^{n-1})^2 + \dots + (2^{n-1})^d = \mathcal{O}(2^{(n-1)d}). \quad (76)$$

□

Here is a slightly more general result than Proposition 1:

Proposition 2. Run the plain BnB (resp. ACM) algorithm with the splitting rule that divides cubes into 2^n (resp. 2^{n-1}) congruent sub-cubes and with the stopping criterion that terminates at the maximal splitting depth d . Additionally, we prune a proportion r of all cubes in each depth. Then the following holds:

- (Perfect Bounds) If at every iteration both ACM and plain BnB prune all sub-cubes except one that contains the global optimum, then ACM needs $\mathcal{O}((1-r)2^{n-1}d)$ iterations to terminate, while plain BnB needs $\mathcal{O}((1-r)2^nd)$.
- (Invalid Bounds) If neither ACM nor plain BnB prunes any sub-cubes at each iteration, then ACM needs $\mathcal{O}(((1-r)2^{n-1})^d)$ iterations to terminate, while plain BnB needs $\mathcal{O}(((1-r)2^n)^d)$.

APPENDIX B

TYPICAL CONSTRAINT AND REFORMULATION ON ANGULAR SEARCH

Consensus maximization problems that search for an angle α typically involve a constraint of the form

$$|a_1 \sin \alpha + a_2 \cos \alpha| \leq c, \quad (77)$$

where α is the optimization variable of the underlying consensus maximization problem, a_1 and a_2 are constants derived from data, and c is a given noise bound. By basic trigonometry, there exist unique angles $\beta_1, \beta_2 \in [-\pi, \pi]$ satisfying

$$\begin{aligned} a_1 \sin \alpha + a_2 \cos \alpha &= \sqrt{a_1^2 + a_2^2} (\sin \beta_1 \sin \alpha + \cos \beta_1 \cos \alpha) \\ &= \sqrt{a_1^2 + a_2^2} \cos(\alpha - \beta_1) \end{aligned} \quad (78)$$

$$\begin{aligned} &= \sqrt{a_1^2 + a_2^2} (\cos \beta_2 \sin \alpha + \sin \beta_2 \cos \alpha) \\ &= \sqrt{a_1^2 + a_2^2} \sin(\alpha + \beta_2). \end{aligned} \quad (79)$$

We can use either (78) or (79) to find the intervals where every α satisfies constraint (77), and the choice can be problem-specific. In the following two subsections, we describe how to solve (78) and (79) for intervals of α , respectively.

B.1 Solved by *cosine* form

Take the TIM constraint as an example. There is a unique angle $\beta_1 \in [-\pi, \pi]$ satisfying

$$\sin \beta_1 = \frac{d_1}{\sqrt{d_1^2 + d_2^2}}, \quad \cos \beta_1 = \frac{d_2}{\sqrt{d_1^2 + d_2^2}}, \quad (80)$$

such that (28) can be rewritten as

$$\begin{aligned} &|\cos(\alpha - \beta_1) + \tilde{d}_3| \leq \tilde{c} \\ \Rightarrow \max\{-1, -\tilde{c} - \tilde{d}_3\} &\leq \cos(\alpha - \beta_1) \leq \min\{1, \tilde{c} - \tilde{d}_3\}, \end{aligned} \quad (81)$$

where $\tilde{c} = \epsilon / \sqrt{d_1^2 + d_2^2}$, $\tilde{d}_3 = d_3 / \sqrt{d_1^2 + d_2^2}$ and denote $c_1 = \max\{-1, -\tilde{c} - \tilde{d}_3\}$ and $c_2 = \min\{1, \tilde{c} - \tilde{d}_3\}$. Notice that $|\alpha - \beta_1| \leq 2\pi$, then to find the interval of α the discussion is separated to 2 situations: 1) $|\alpha - \beta_1| \leq \pi$ and 2) $\pi \leq |\alpha - \beta_1| \leq 2\pi$.

1) when $|\alpha - \beta_1| \leq \pi$, since *arccosine* function is descending (81) is equivalent to

$$\begin{aligned} \arccos c_2 &\leq |\alpha - \beta_1| \leq \arccos c_1 \\ (c_3 := \arccos c_2 \text{ and } c_4 := \arccos c_1) \\ \Rightarrow \alpha &\in ([\beta_1 - c_4, \beta_1 - c_3] \cup [\beta_1 + c_3, \beta_1 + c_4]) \cap [-\pi, \pi] \end{aligned} \quad (82)$$

2) when $\pi \leq |\alpha - \beta_1| \leq 2\pi$, notice that $\cos(2\pi - \beta) = \cos \beta$ and $|2\pi - (\alpha - \beta_1)| \leq \pi$, then similarly (81) is equivalent to

$$\begin{aligned} \alpha &\in ([\beta_1 - 2\pi + c_3, \beta_1 - 2\pi + c_4] \\ &\cup [\beta_1 + 2\pi - c_4, \beta_1 + 2\pi - c_3]) \cap [-\pi, \pi]. \end{aligned} \quad (83)$$

To sum up, (81) requires the yaw angle $\alpha \in [-\pi, \pi]$ lie in the union of (82, 83).

B.2 Solved by *sine* form

In *sine* form, there is a unique angle $\beta_2 \in [-\pi, \pi]$ satisfying

$$\sin \beta_2 = \frac{d_2}{\sqrt{d_1^2 + d_2^2}}, \quad \cos \beta_2 = \frac{d_1}{\sqrt{d_1^2 + d_2^2}} \quad (84)$$

such that (77) can be rewritten as

$$\begin{aligned} &|\sin(\alpha + \beta_2)| \leq \tilde{c} \\ \Rightarrow \max\{-1, -\tilde{c}\} &\leq \sin(\alpha + \beta_2) \leq \min\{1, \tilde{c}\}, \end{aligned} \quad (85)$$

where $\tilde{c} = c / \sqrt{a_1^2 + a_2^2}$. Notice that $|\alpha + \beta_2| \leq 2\pi$ and denote $c_5 = \arcsin \max\{-1, -\tilde{c}\}$ and $c_6 = \arcsin \min\{1, \tilde{c}\}$, then to find the interval of α the discussion is separated to 5 situations:

1) when $|\alpha + \beta_2| \leq \frac{\pi}{2}$, since *arcsine* function is ascending then

$$\alpha \in [c_5 - \beta_2, c_6 - \beta_2] \cap [-\pi, \pi]$$

2) when $\frac{\pi}{2} \leq \alpha + \beta_2 \leq \frac{3\pi}{2}$, since $\sin \beta = -\sin(\beta - \pi)$ then

$$\alpha \in [\pi - c_6 - \beta_2, \pi - c_5 - \beta_2] \cap [-\pi, \pi]$$

3) when $-\frac{3\pi}{2} \leq \alpha + \beta_2 \leq \frac{\pi}{2}$, since $\sin \beta = -\sin(\beta + \pi)$ then

$$\alpha \in [-\pi - c_6 - \beta_2, -\pi - c_5 - \beta_2] \cap [-\pi, \pi]$$

4) when $\frac{3\pi}{2} \leq \alpha + \beta_2 \leq 2\pi$, since $\sin \beta = \sin(\beta - 2\pi)$ then

$$\alpha \in [2\pi + c_5 - \beta_2, 2\pi + c_6 - \beta_2] \cap [-\pi, \pi]$$

5) when $-2\pi \leq \alpha + \beta_2 \leq -\frac{3\pi}{2}$, since $\sin \beta = \sin(\beta + 2\pi)$ then

$$\alpha \in [-2\pi + c_5 - \beta_2, -2\pi + c_6 - \beta_2] \cap [-\pi, \pi]$$

To sum up, (85) requires the angle $\alpha \in [-\pi, \pi]$ to lie in the union of the above intervals. The above results can be used to solve the Planar Motion problem (38) by ACM-1.

APPENDIX C

ELABORATION ON REMARK 1

Definition 2. The diameter of a cube $\mathcal{C} \subset \mathbb{R}^n$ defined in (3.2) is

$$\delta(\mathcal{C}) = \sqrt{(c_1^r - c_1^l)^2 + \dots + (c_n^r - c_n^l)^2}. \quad (86)$$

Suppose all sides of the initial cube have equal lengths L_0 , then the smallest cube that BnB terminates on also has equal length sides. Denote the maximal depth for plain BnB and ACM-X as d_1 and d_2 respectively, and the minimal sub-cube of plain BnB and ACM-X as \mathcal{C}_1 and \mathcal{C}_2 respectively. Then we can get

$$\delta(\mathcal{C}_1) = \frac{\sqrt{n}}{2^{d_1}} L_0, \quad \delta(\mathcal{C}_2) = \frac{\sqrt{n-1}}{2^{d_2}} L_0. \quad (87)$$

Let ACM-X has the same minimal diameter as plain BnB

$$\delta(\mathcal{C}_1) = \delta(\mathcal{C}_2) \Rightarrow d_2 = d_1 + \log_2 \frac{\sqrt{n-1}}{\sqrt{n}}. \quad (88)$$

For $n \geq 2$,

$$-0.5 \leq \log_2 \frac{\sqrt{n-1}}{\sqrt{n}} < 0. \quad (89)$$

Therefore, we can get $d_1 - 0.5 \leq d_2 < d_1$, then the same diameter tolerance approximately implies the same maximal depth.

Example 4. Set the maximal depth $d_1 = d_2 = 10$ and $L_0 = 1$, then the minimal diameter difference between BnB and ACM-X is

$$0 \leq \frac{\sqrt{n}}{2^{10}} - \frac{\sqrt{n-1}}{2^{10}} \leq 4.05 \times 10^{-4}. \quad (90)$$

APPENDIX D

LOWER AND UPPER BOUNDS OF ACM-2 CORR

Here we provide details on the lower and upper bounds of ACM-2 Corr for 3D-3D correspondence-based registration.

Recall (51) provides an equivalent interval of $h(\mathbf{t}) \leq \epsilon$

$$h(\mathbf{t}) \leq \epsilon \Leftrightarrow (\|\mathbf{q}_i\|_2 - \epsilon)^2 \leq \|\mathbf{p}_i + \mathbf{t}\|_2^2 \leq (\|\mathbf{q}_i\|_2 + \epsilon)^2, \quad (91)$$

and denote $c_{i1} = (\|\mathbf{q}_i\|_2 - \epsilon)^2$ and $c_{i2} = (\|\mathbf{q}_i\|_2 + \epsilon)^2$ for the sake of simplification. And notice that $\|\mathbf{p}_i + \mathbf{t}\|_2^2$ can be separate as two parts: $h_1(t_1, t_2) = (p_{1i} + t_1)^2 + (p_{2i} + t_2)^2$ and $h_2(t_3) = (p_{3i} + t_3)^2$.

For the lower bound of ACM-2, given then centre point of $\mathcal{C}_{ACM} [t_1^c, t_2^c]^T$, an interval of t_3 can be derived as follows

$$|h_i(t_1^c, t_2^c; t_3)| \leq \epsilon \quad (92)$$

$$\Leftrightarrow c_{i1} - h_1(t_1^c, t_2^c) \leq (p_{3i} + t_3)^2 \leq c_{i2} - h_1(t_1^c, t_2^c) \quad (93)$$

$$\Leftrightarrow c_{i3} \leq p_{3i} + t_3 \leq c_{i4} \quad (94)$$

$$\Leftrightarrow t_3 \in [c_{i3} - p_{3i}, c_{i4} - p_{3i}], \quad (95)$$

where

$$c_{i3} = \sqrt{\max\{0, c_{i1} - h_1(t_1^c, t_2^c)\}} \quad (96)$$

$$c_{i4} = \sqrt{\max\{0, c_{i2} - h_1(t_1^c, t_2^c)\}}. \quad (97)$$

Then the lower bound of ACM-2 Corr can be obtained by using Interval Stabbing to solve the follows

$$\begin{aligned} L(\mathcal{C}_{ACM}) &= \max_{t_3} \sum_i \mathbf{1}(|h_i(t_1^c, t_2^c; t_3)| < \epsilon) \\ &= \max_{t_3} \sum_i \mathbf{1}(t_3 \in [c_{i3} - p_{3i}, c_{i4} - p_{3i}]). \end{aligned} \quad (98)$$

Now consider the upper bound of ACM-2 Corr. For a pair of 3D-3D correspondence $(\mathbf{p}_i, \mathbf{q}_i)$, an interval of $h_1(t_1, t_2)$ on \mathcal{C}_{ACM} can be calculated. Denote the interval as $h_1(\mathcal{C}_{ACM}) \in [h_{1i}^l, h_{1i}^r]$. Then $|h(\mathcal{C}_{ACM})| \leq \epsilon$ is a relaxation of the constraint $|h(\mathbf{t})| \leq \epsilon$. And we can get the following interval of t_3

$$|h(\mathcal{C}_{ACM})| \leq \epsilon \quad (99)$$

$$\Leftrightarrow c_{i1} - h_{1i}^l \leq c_{i2} - h_{1i}^r \quad (100)$$

$$\Leftrightarrow c_{i5} \leq p_{3i} + t_3 \leq c_{i5} \quad (101)$$

$$\Leftrightarrow t_3 \in [c_{i5} - p_{3i}, c_{i6} - p_{3i}], \quad (102)$$

where

$$c_{i5} = \sqrt{\max\{0, c_{i1} - h_{1i}^l\}} \quad (103)$$

$$c_{i6} = \sqrt{\max\{0, c_{i2} - h_{1i}^r\}}. \quad (104)$$

Therefore, the upper bound of ACM-2 Corr can be obtained by using Interval Stabbing to solve the follows

$$\begin{aligned} U(\mathcal{C}_{ACM}) &= \max_{t_3} \sum_i \mathbf{1}(|h_i(\mathcal{C}_{ACM}; t_3)| < \epsilon) \\ &= \max_{t_3} \sum_i \mathbf{1}(t_3 \in [c_{i5} - p_{3i}, c_{i6} - p_{3i}]). \end{aligned} \quad (105)$$

APPENDIX E

ELABORATION ON REMARK 2

We can rewrite (58) in a similar manner like (59)

$$\max_{\mathbf{t}} \sum_m \sum_n \mathbf{1}(\|\mathbf{F}_{m,n}(\mathbf{t})\|_\infty < \epsilon). \quad (106)$$

Notice that we can define an auxiliary function $h_m(\mathbf{t})$ to decompose the objective in (106) as follows

$$\begin{aligned} &\sum_m \sum_n \mathbf{1}(\|\mathbf{F}_{m,n}(\mathbf{t})\|_\infty < \epsilon) \\ &= \sum_m \left(\max_n \mathbf{1}(\|\mathbf{F}_{m,n}(\mathbf{t})\|_\infty < \epsilon) + h_m(\mathbf{t}) \right). \end{aligned} \quad (107)$$

For every m when there is multiple n such that $\|\mathbf{F}_{m,n}(\mathbf{t})\|_\infty < \epsilon$ then $h_m(\mathbf{t}) > 0$ and otherwise $h_m(\mathbf{t}) = 0$. For a proper noise bound ϵ , it is always true that there is only one pair (i, j) such that

$$\|\mathbf{q}_i\| - \|\mathbf{p}_j + \mathbf{t}^*\| < \epsilon. \quad (108)$$

That means when (106) converge to an optimal solution \mathbf{t}^* , $h_m(\mathbf{t}^*) = 0$ for all m . Therefore,

$$\begin{aligned} &\sum_m \sum_n \mathbf{1}(\|\mathbf{F}_{m,n}(\mathbf{t}^*)\|_\infty < \epsilon) \\ &= \sum_m \max_n \mathbf{1}(\|\mathbf{F}_{m,n}(\mathbf{t}^*)\|_\infty < \epsilon) \\ &\Rightarrow \max_{\mathbf{t}} \sum_m \sum_n \mathbf{1}(\|\mathbf{F}_{m,n}(\mathbf{t})\|_\infty < \epsilon) \\ &= \max_{\mathbf{t}} \sum_m \max_n \mathbf{1}(\|\mathbf{F}_{m,n}(\mathbf{t})\|_\infty < \epsilon). \end{aligned} \quad (109)$$

REFERENCES

- [1] M. A. Fischler and R. C. Bolles, "Random sample consensus: a paradigm for model fitting with applications to image analysis and automated cartography," *Communications of the ACM*, vol. 24, no. 6, pp. 381–395, 1981. [1, 2](#)
- [2] H. Li, "Consensus set maximization with guaranteed global optimality for robust geometry estimation," in *Proceedings of the International Conference on Computer Vision (ICCV)*. IEEE, 2009, pp. 1074–1080. [2, 3](#)
- [3] T.-J. Chin, P. Purkait, A. Eriksson, and D. Suter, "Efficient globally optimal consensus maximisation with tree search," in *Proceedings of the IEEE Conference on Computer Vision and Pattern Recognition (CVPR)*. Boston, MA, USA: IEEE, 2015, pp. 2413–2421. [2, 3](#)
- [4] Z. Cai, T.-J. Chin, H. Le, and D. Suter, "Deterministic consensus maximization with biconvex programming," in *Proceedings of the European Conference on Computer Vision (ECCV)*, 2018, pp. 685–700. [2, 3](#)
- [5] L. Kneip and P. Furgale, "Opengv: A unified and generalized approach to real-time calibrated geometric vision," in *Proceedings of the IEEE International Conference on Robotics and Automation (ICRA)*. IEEE, 2014, pp. 1–8. [2, 9](#)
- [6] P. Torr and A. Zisserman, "MLESAC: A New Robust Estimator with Application to Estimating Image Geometry," *Computer Vision and Image Understanding (CVIU)*, vol. 78, no. 1, pp. 138–156, 2000. [2](#)
- [7] D. Nistér, "Preemptive ransac for live structure and motion estimation," in *Proceedings of the IEEE Conference on Computer Vision and Pattern Recognition (CVPR)*, 2003, pp. 199–206. [2](#)
- [8] O. Chum, J. Matas, and J. Kittler, "Locally optimized ransac," in *In Joint Pattern Recognition Symposium*, 2003. [2](#)
- [9] A. Chum and J. Matas, "Matching with PROSAC – Progressive Sample Consensus," in *Proceedings of the IEEE Conference on Computer Vision and Pattern Recognition (CVPR)*, 2005. [2](#)
- [10] D. Barath and J. Matas, "Graph-cut ransac," in *Proceedings of the IEEE Conference on Computer Vision and Pattern Recognition (CVPR)*, 2018, pp. 6733–6741. [2](#)

- [11] C. Olsson, F. Kahl, and M. Oskarsson, "Optimal estimation of perspective camera pose," in *Proceedings of the International Conference on Pattern Recognition (ICPR)*, Hong Kong, China, 2006. [2](#)
- [12] R. Hartley and F. Kahl, "Global optimization through searching rotation space and optimal estimation of the essential matrix," in *Proceedings of the International Conference on Computer Vision (ICCV)*, 2007. [2](#)
- [13] —, "Global optimization through rotation space search," *International Journal of Computer Vision (IJCV)*, vol. 82, pp. 64–79, 2009. [2, 3](#)
- [14] C. Olsson, F. Kahl, and M. Oskarsson, "Branch and bound methods for euclidean registration problems," *IEEE Transactions on Pattern Analysis and Machine Intelligence (PAMI)*, vol. 31, no. 5, pp. 783–794, 2008. [2](#)
- [15] J. Briaies, L. Kneip, and J. Gonzalez-Jimenez, "A certifiably globally optimal solution to the non-minimal relative pose problem," in *Proceedings of the IEEE Conference on Computer Vision and Pattern Recognition (CVPR)*, Salt Lake City, US, 2018. [3](#)
- [16] J. Zhao, W. Xu, and L. Kneip, "A certifiably globally optimal solution to generalized essential matrix estimation," in *Proceedings of the IEEE Conference on Computer Vision and Pattern Recognition (CVPR)*, Seattle, USA, 2020. [3](#)
- [17] F. Kahl, S. Agarwal, M. Chandraker, D. Kriegman, and S. Belongie, "Practical global optimization for multiview geometry," *International Journal of Computer Vision (IJCV)*, vol. 79, no. 3, pp. 271–284, 2008. [3](#)
- [18] J. Bazin, Y. Seo, and M. Pollefeys, "Globally optimal consensus set maximization through rotation search," in *Proceedings of the Asian Conference on Computer Vision (ACCV)*. Springer, 2012, pp. 539–551. [3](#)
- [19] J. Bazin, Y. Seo, R. Hartley, and M. Pollefeys, "Globally optimal inlier set maximization with unknown rotation and focal length," in *Proceedings of the European Conference on Computer Vision (ECCV)*, 2014. [3](#)
- [20] H. Li, P. Kim, J. Zhao, K. Joo, Z. Cai, Z. Liu, and Y.-H. Liu, "Globally optimal and efficient vanishing point estimation in atlanta world," in *Proceedings of the European Conference on Computer Vision (ECCV)*. Springer, 2020, pp. 153–169. [3, 5](#)
- [21] J. Yang, H. Li, and Y. Jia, "Optimal essential matrix estimation via inlier-set maximization," in *Proceedings of the European Conference on Computer Vision (ECCV)*, 2014. [3](#)
- [22] A. Bustos and T.-J. Chin, "Guaranteed outlier removal for point cloud registration with correspondences," *IEEE Transactions on Pattern Analysis and Machine Intelligence (PAMI)*, vol. 40, no. 12, pp. 2868–2882, 2017. [3, 5](#)
- [23] P. Speciale, D. Paudel, M. Oswald, T. Kroeger, L. Van Gool, and M. Pollefeys, "Consensus maximization with linear matrix inequality constraints," in *Proceedings of the IEEE Conference on Computer Vision and Pattern Recognition (CVPR)*, 2017, pp. 4941–4949. [3](#)
- [24] Y. Liu, G. Chen, R. Gu, and A. Knoll, "Globally Optimal Consensus Maximization for Relative Pose Estimation With Known Gravity Direction," vol. 6, no. 3, pp. 5905–5912, 2021. [3](#)
- [25] Y. Jiao, Y. Wang, X. Ding, M. Wang, and R. Xiong, "Deterministic Optimality for Robust Vehicle Localization Using Visual Measurements," *IEEE Transactions on Intelligent Transportation Systems (ITS)*, pp. 1–14, 2021. [3, 5](#)
- [26] H. Liu, G. Chen, Y. Liu, Z. Liang, R. Zhang, and A. Knoll, "Globally-optimal inlier maximization for relative pose estimation under planar motion," *Frontiers in Neurorobotics*, vol. 16, 2022. [3, 9, 10](#)
- [27] Y. Jiao, Y. Wang, B. Fu, Q. Tan, L. Chen, M. Wang, S. Huang, and R. Xiong, "Globally optimal consensus maximization for robust visual inertial localization in point and line map," in *2020 IEEE/RSJ International Conference on Intelligent Robots and Systems (IROS)*. IEEE, pp. 4631–4638. [3, 5, 8, 9](#)
- [28] T. Breuel, "Implementation techniques for geometric branch-and-bound matching methods," *Computer Vision and Image Understanding (CVIU)*, vol. 90, no. 3, pp. 258–294, 2003. [3, 4](#)
- [29] J. Yang, H. Li, and Y. Jia, "Go-ICP: Solving 3D Registration Efficiently and Globally Optimally," in *Proceedings of the International Conference on Computer Vision (ICCV)*, 2013. [3](#)
- [30] J. Yang, H. Li, D. Campbell, and Y. Jia, "Go-ICP: A Globally Optimal Solution to 3D ICP Point-Set Registration," *IEEE Transactions on Pattern Analysis and Machine Intelligence (PAMI)*, vol. 38, no. 11, pp. 2241–2254, 2016. [3](#)
- [31] A. Bustos, T.-J. Chin, and D. Suter, "Fast rotation search with stereographic projections for 3d registration," in *Proceedings of the IEEE Conference on Computer Vision and Pattern Recognition (CVPR)*, 2014, pp. 3930–3937. [3, 13](#)
- [32] Y. Liu, C. Wang, Z. Song, and M. Wang, "Efficient global point cloud registration by matching rotation invariant features through translation search," in *Proceedings of the European Conference on Computer Vision (ECCV)*, 2018, pp. 448–463. [3, 12, 13, 14, 15](#)
- [33] H. Yang and L. Carlone, "A polynomial-time solution for robust registration with extreme outlier rates," *arXiv preprint arXiv:1903.08588*, 2019. [3, 5](#)
- [34] H. Yang, J. Shi, and L. Carlone, "Teaser: Fast and certifiable point cloud registration," *IEEE Transactions on Robotics (T-RO)*, vol. 37, no. 2, pp. 314–333, 2020. [3, 5, 12](#)
- [35] Z. Cai, T.-J. Chin, A. Bustos, and K. Schindler, "Practical optimal registration of terrestrial lidar scan pairs," *ISPRS journal of photogrammetry and remote sensing*, vol. 147, pp. 118–131, 2019. [3, 5](#)
- [36] L. Peng, M. Tsakiris, and R. Vidal, "Arcs: Accurate rotation and correspondence search," in *Proceedings of the IEEE Conference on Computer Vision and Pattern Recognition (CVPR)*, 2022, pp. 11 153–11 163. [3, 5, 13](#)
- [37] D. Campbell, L. Petersson, L. Kneip, and H. Li, "Globally-optimal inlier set maximisation for simultaneous camera pose and feature correspondence," in *Proceedings of the International Conference on Computer Vision (ICCV)*, 2017, pp. 1–10. [3](#)
- [38] D. Campbell, L. Petersson, L. Kneip, and H. Li, "Globally-optimal inlier set maximisation for camera pose and correspondence estimation," *IEEE Transactions on Pattern Analysis and Machine Intelligence (PAMI)*, vol. 42, pp. 328–342, 2020. [3](#)
- [39] D. Campbell, L. Petersson, L. Kneip, H. Li, and S. Gould, "The alignment of the spheres: Globally-optimal spherical mixture alignment for camera pose estimation," in *Proceedings of the IEEE Conference on Computer Vision and Pattern Recognition (CVPR)*, 2019. [3](#)
- [40] L. Hu and L. Kneip, "Globally optimal point set registration by joint symmetry plane fitting," *Journal of Mathematical Imaging and Vision (JMIV)*, vol. 63, pp. 689–707, 2021. [3](#)
- [41] L. Gao, J. Su, J. Cui, X. Zeng, X. Peng, and L. Kneip, "Efficient globally-optimal correspondence-less visual odometry for planar ground vehicles," in *Proceedings of the IEEE International Conference on Robotics and Automation (ICRA)*, 2020. [3](#)
- [42] X. Peng, Y. Wang, L. Gao, and L. Kneip, "Globally-optimal event camera motion estimation," in *Proceedings of the European Conference on Computer Vision (ECCV)*, 2020. [3](#)
- [43] X. Peng, L. Gao, Y. Wang, and L. Kneip, "Globally-optimal contrast maximisation for event cameras," *IEEE Transactions on Pattern Analysis and Machine Intelligence (PAMI)*, vol. 44, no. 7, pp. 3479–3495, 2021. [3](#)
- [44] Z. Cai, T.-J. Chin, and V. Koltun, "Consensus Maximization Tree Search Revisited," in *Proceedings of the International Conference on Computer Vision (ICCV)*, Seoul, Korea (South), 2019, pp. 1637–1645. [3](#)
- [45] Z. Cai, "Consensus Maximization: Theoretical Analysis and New Algorithms," Ph.D. dissertation, University of Adelaide, 2020. [3](#)
- [46] T.-J. Chin, Z. Cai, and F. Neumann, "Robust fitting in computer vision: Easy or hard?" *International Journal of Computer Vision (IJCV)*, vol. 128, no. 3, pp. 575–587, 2020. [3](#)
- [47] D. Scholz, *Deterministic global optimization: geometric branch-and-bound methods and their applications*. Springer Science & Business Media, 2011, vol. 63. [3, 8](#)
- [48] M. Berg, M. Kreveld, M. Overmars, and O. Schwarzkopf, "Computational geometry," in *Computational geometry*. Springer, 1997, pp. 1–17. [5](#)
- [49] J. Clausen, "Branch and bound algorithms-principles and examples," *Department of Computer Science, University of Copenhagen*, pp. 1–30, 1999. [8](#)
- [50] A. Geiger, P. Lenz, C. Stiller, and R. Urtasun, "Vision meets robotics: The kitti dataset," *The International Journal of Robotics Research*, vol. 32, no. 11, pp. 1231–1237, 2013. [11](#)
- [51] D. G. Lowe, "Distinctive image features from scale-invariant keypoints," *International journal of computer vision*, vol. 60, pp. 91–110, 2004. [11](#)
- [52] B. Curless and M. Levoy, "A volumetric method for building complex models from range images," in *Proceedings of the 23rd annual conference on Computer graphics and interactive techniques*, 1996, pp. 303–312. [14](#)

- [53] F. Pomerleau, F. Colas, R. Siegwart, and S. Magnenat, “Comparing icp variants on real-world data sets: Open-source library and experimental protocol,” *Autonomous Robots*, vol. 34, pp. 133–148, 2013. [14](#)
- [54] Z. Zhang, C. Fu, C. Dong, C. Mertz, and J. M. Dolan, “Self-calibration of multiple lidars for autonomous vehicles,” in *2021 IEEE International Intelligent Transportation Systems Conference (ITSC)*. IEEE, 2021, pp. 2897–2902. [15](#)